



**HAL**  
open science

## Partial melting of a C-rich asteroid: Lithophile trace elements in ureilites

Jean-Alix J-A Barrat, Albert Jambon, Akira Yamaguchi, Addi Bischoff, Marie-Laure Rouget, Céline C. Liorzou

### ► To cite this version:

Jean-Alix J-A Barrat, Albert Jambon, Akira Yamaguchi, Addi Bischoff, Marie-Laure Rouget, et al.. Partial melting of a C-rich asteroid: Lithophile trace elements in ureilites. *Geochimica et Cosmochimica Acta*, 2016, 194, pp.163-178. 10.1016/j.gca.2016.08.042 . hal-01365231

**HAL Id: hal-01365231**

**<https://hal.sorbonne-universite.fr/hal-01365231>**

Submitted on 14 Sep 2016

**HAL** is a multi-disciplinary open access archive for the deposit and dissemination of scientific research documents, whether they are published or not. The documents may come from teaching and research institutions in France or abroad, or from public or private research centers.

L'archive ouverte pluridisciplinaire **HAL**, est destinée au dépôt et à la diffusion de documents scientifiques de niveau recherche, publiés ou non, émanant des établissements d'enseignement et de recherche français ou étrangers, des laboratoires publics ou privés.

1 **Partial melting of a C-rich asteroid:**  
2 **Lithophile trace elements in ureilites.**

3 by

4 Jean-Alix Barrat<sup>1</sup>, Albert Jambon<sup>2</sup>, Akira Yamaguchi<sup>3</sup>,  
5 Addi Bischoff<sup>4</sup>, Marie-Laure Rouget<sup>5</sup>, and Céline Liorzou<sup>1</sup>

6  
7 1: Université de Bretagne Occidentale, Institut Universitaire Européen de la Mer, CNRS UMR 6538, Place  
8 Nicolas Copernic, 29280 Plouzané, France. E-mail : [barrat@univ-brest.fr](mailto:barrat@univ-brest.fr)

9 2: Sorbonne Universités, UPMC Univ Paris 06, UMR 7193, Institut des Sciences de la Terre Paris (iSTeP),  
10 F-75005 Paris, France.

11  
12 3: National Institute of Polar Research, Tachikawa, Tokyo 190-8518, Japan and Department of Polar  
13 Science, School of Multidisciplinary Science, Graduate University for Advanced Sciences, Tachikawa,  
14 Tokyo 190-8518, Japan

15 4: Institut für Planetologie, Westfälische Wilhelms-Universität Münster, Wilhelm-Klemm-Str. 10, 48149  
16 Münster, Germany.

17 5: Université de Bretagne Occidentale, Institut Universitaire Européen de la Mer, CNRS UMS 3113, Place  
18 Nicolas Copernic, 29280 Plouzané Cedex, France.

19  
20  
21 Keywords: trace elements, achondrite, ureilite, partial melting

22  
23  
24  
25  
26 submitted to *Geochimica et Cosmochimica Acta*, 27/04/2016

27 in press, 29/08/2016

29 **Abstract**

30 Ureilites are among the most common achondrites and are widely believed to sample the mantle of a  
31 single, now-disrupted, C-rich body. We analyzed 17 ureilite samples, mostly Antarctic finds, and determined  
32 their incompatible trace element abundances. In order to remove or reduce the terrestrial contamination,  
33 which is marked among Antarctic ureilites by light-REE enrichment, we leached the powdered samples with  
34 nitric acid. The residues display consistent abundances, which strongly resemble those of the pristine rocks.  
35 All the analyzed samples display light-REE depletions, negative Eu anomalies, low  $(\text{Sr}/\text{Eu}^*)_n$ , and  $(\text{Zr}/\text{Eu}^*)_n$   
36 ratios which are correlated. Two groups of ureilites (groups A and B) are defined. Compared to group A,  
37 group B ureilites, which are the less numerous, tend to be richer in heavy REEs, more light-REE depleted,  
38 and display among the deepest Eu anomalies. In addition, olivine cores in group B ureilites tend to be more  
39 forsteritic ( $\text{Mg}\# = 81.9\text{-}95.2$ ) than in group A ureilites ( $\text{Mg}\# = 74.7\text{-}86.1$ ). Incompatible trace element  
40 systematics supports the view that ureilites are mantle restites. REE modelling suggests that their precursors  
41 were rather REE-rich (ca.  $1.8\text{-}2 \times \text{CI}$ ) and contained a phosphate phase, possibly merrillite. The REE  
42 abundances in ureilites can be explained if at least two distinct types of magmas were removed successively  
43 from their precursors: aluminous and alkali-rich melts as exemplified by the Almahata Sitta trachyandesite  
44 (ALM-A), and Al and alkali-poor melts produced after the exhaustion of plagioclase from the source. Partial  
45 melting was near fractional (group B ureilites, which are probably among the least residual samples) to  
46 dynamic with melt porosities that did not exceed a couple of percent (group A ureilites). The ureilite parent  
47 body (UPB) was almost certainly covered by a crust formed chiefly from the extrusion products of the  
48 aluminous and alkali-rich magmas. It is currently uncertain whether the Al and alkali-poor melts produced  
49 during the second phase of melting reached the surface of the body. The fact that initial silicate melting of  
50 ureilitic precursors would have produced relatively low density liquids capable of forming an external crust  
51 to the UPB casts doubt on models that invoke chondritic outer layers to achondritic asteroids.

## 1. Introduction

The early history of the Solar System was marked by the accretion of numerous asteroid-sized bodies (large asteroids and embryos). Many of them underwent rapid internal heating, leading to melting and subsequent differentiation. Among the most significant issues for understanding the differentiation of rocky bodies are the exact processes of melting, the compositions of the generated magmas and how these were then segregated from their sources. Melt migration may have involved ascent to the surface to form a crust, or alternatively escape to space by explosive volcanism. It has recently been argued that partial melting of carbonaceous chondrite-like bodies (e.g. CV or CM), could have produced melts too dense to erupt through buoyancy alone. Consequently, the differentiation of such bodies could have generated distinctive internal structures, with a preserved chondritic carapace at the surface covering an igneous layer, and possibly a metallic core at their centers (Weiss and Elkins-Tanton, 2013; Fu and Elkins-Tanton, 2014). If true, these bodies could have harbored magnetic dynamos when their cores were still molten. The discovery that some CM and CV chondrites recorded ancient magnetic fields has strengthened such a view, although the origin of these fields, whether internal or linked to an early stage of solar activity, remains a matter for debate (e.g. Carporzen et al., 2011; Cournède et al., 2015).

The structure and differentiation history of C-rich bodies can be studied directly using meteorite samples. Unfortunately, no representative sampling of a single body, i.e. from the core to the crust, is currently available. However, the ureilites, one of the largest families of achondrites (ca. 400 different meteorites and 17 % of the known achondrites currently reported in the Meteoritical Bulletin Database), represent a unique collection from the mantle of a single, now-disrupted, C-rich body (Downes et al., 2008). These rocks are coarse-grained peridotites, consisting chiefly of olivine and pyroxene (pigeonite, and more rarely augite and orthopyroxene), abundant carbon (up to 7 wt%, graphite and diamond), with accessory metal and sulfides (e.g., Mittlefehldt et al., 1998). It is noteworthy that these peridotites are virtually devoid of feldspar.

Ureilites have been the focus of many geochemical studies. Even though uncertainties remain concerning the differentiation of the UPB, thermal modeling and extinct isotope systematics make it possible to reconstruct its overall history (e.g., Wilson et al., 2008; Budde et al., 2015; Goodrich et al., 2015). It accreted no more than 1.6 Ma after CAIs, i.e. later than the parent bodies of the magmatic irons, and about half a million years before most of the chondrite parent bodies. The UPB was definitely C-rich, but was isotopically distinct from the carbonaceous chondrites (Yamakawa et al., 2010; Warren, 2011). However, it contained enough  $^{26}\text{Al}$  to be heated by the decay of this isotope, which allowed the segregation of S-rich metallic melts (e.g., Warren et al., 2006; Rankenburg et al., 2008; Budde et al., 2015), more likely before the onset of silicate melting (Barrat et al., 2015). Subsequent extraction of silicate melts is demonstrated by the presence of feldspar-rich rock debris in ureilitic breccias (e.g., Ikeda et al., 2000; Cohen et al., 2004; Bischoff et al., 2014), but the melting experienced by the UPB was more limited than in other early bodies,

91 such as the angrite parent body or Vesta, where magma oceans homogenized the O isotope compositions  
92 (Greenwood et al., 2005). Indeed, ureilites display a wide range of  $\Delta^{17}\text{O}$  values which are well correlated  
93 with various mineral compositions (Clayton and Mayeda, 1996, and Fig. 1). Systematics of short-lived  
94 isotopes ( $^{53}\text{Mn}$ - $^{53}\text{Cr}$ ,  $^{182}\text{Hf}$ - $^{182}\text{W}$ ,  $^{26}\text{Al}$ - $^{26}\text{Mg}$ ) indicate that the differentiation occurred between 3 and 7 Ma  
95 after the CAIs (Yamakawa et al., 2010; Goodrich et al., 2010, Bischoff et al., 2014; Budde et al., 2015). It  
96 stopped soon after, with the catastrophic breakup of the body following a large impact, while its mantle was  
97 still hot.

98

99 Although it is now widely accepted that most ureilites are mantle restites (e.g., Boynton et al., 1976;  
100 Takeda, 1987; Warren and Kallemeyn, 1992; Scott et al., 1993; Warren et al., 2006; Goodrich et al., 2015  
101 among others), the melting processes and the involvement of C during their formation are matters of intense  
102 debate. During the ureilite disruption event, C locally reduced olivine crystals, and produced their distinctive  
103 iron-depleted rims and veins (e.g., Miyamoto et al., 1985). Except for these rims and veins, olivines are quite  
104 uniform in Mg# number [=100Mg/(Mg +Fe), atomic] within any given ureilite. However, between different  
105 samples their compositions display a huge variation, as shown by the olivine-core Mg# (=forsterite content),  
106 which range from 74 to 97. The Fe/Mn ratios (ranging from 3 to 57) are correlated with this parameter (e.g.,  
107 Clayton and Mayeda, 1996; Mittlefehldt et al., 1998, Fig. 1). A similar relationship is also shown by  
108 pyroxenes, which are in equilibrium with the olivines. It has been often proposed that varying degrees of  
109 partial reduction coincident with partial melting (a process named “smelting”) produced the range of olivine  
110 (and pyroxene) core compositions, from an initial proto-ureilitic material, displaying a near-uniform olivine-  
111 core Mg# number (e.g., Goodrich, 1992; Singletary and Grove, 2003). Alternatively, the diversity of the  
112 silicate compositions could be inherited from the pre-igneous (nebular) history of the accreted materials [see  
113 Warren and Huber (2006), Warren (2012) and Goodrich et al. (2007, 2013a) for extensive discussions of  
114 these models].

115

116 In this paper, we report on trace element abundances obtained by Inductively Coupled Plasma Mass  
117 Spectrometry (ICP-MS) of a suite of unbrecciated ureilites. Our aim is to evaluate the full range of refractory  
118 lithophile element distributions displayed by these meteorites, in order to model the partial melting processes  
119 that occurred in the mantle of the ureilite parent body (UPB) and to discuss the diversity of the melts and  
120 also the possible structure of this C-rich body.

121

## 122 **2. Samples and analytical procedures**

123 We analyzed 15 Antarctic ureilites kindly provided by the NASA meteorite working group (MWG)  
124 and the National Institute of Polar Research (NIPR), and an additional 2 from the Sahara. The details of the  
125 meteorite samples used in this study are given in Table 1. These samples are among the least weathered  
126 ureilitic finds and their olivine cores cover nearly the full range of compositions known for these meteorites  
127 (Fo = 74 to 95 %). One of the samples is anomalous. Unlike other samples which are peridotites, MET

128 01085 is a pyroxenite devoid of olivine. Notice that we do not include in our study polymict ureilites nor  
129 samples of the rare “Hughes” group ureilites.

130 Fragments were crushed to a fine powder using a boron carbide mortar and pestle. Splits of the  
131 powders (typically 200-250 mg) were leached in 4 M HNO<sub>3</sub> at room temperature during 30 minutes (“R1”  
132 residues; two distinct splits of GRO 95575 were independently leached) before dissolution. A subsample of  
133 NWA 8049 (“R2” residue) was leached for 90 minutes under the same conditions in order to evaluate the  
134 effects of a longer leaching duration. MET 01085, which is devoid of olivine, was leached at 120 °C during  
135 30 minutes (“R3” residue). Residues were rinsed twice in ultrapure water and dried before weighing.  
136 Powders (unleached powders and residues) were digested by sequential mixtures of HF/HNO<sub>3</sub>, HNO<sub>3</sub> and  
137 HCl. Elemental abundances were determined using a high-resolution inductively coupled plasma-mass  
138 spectrometer Thermo Element 2 at Institut Universitaire Européen de la Mer (IUEM), Plouzané, following a  
139 well-established procedure (e.g., Barrat et al., 2012). For the residues, Rare Earth Elements (REE) were  
140 separated and concentrated (Barrat et al., 1996) in order to improve the quality of the analyses. Results on  
141 international standards (BCR-2, BIR-1, WS-E, Allende USNM 3529, UB-N, PCC-1) have been repeatedly  
142 reported (Barrat et al., 2012, 2014, 2016). Based on standards and many sample duplicates, the precisions for  
143 abundances and trace element ratios [e.g., Eu/Eu\*, where Eu\* is the expected Eu concentration for a smooth  
144 CI-normalized REE pattern, such that  $Eu_n = (Sm_n \times Gd_n)^{1/2}$ ] are in most cases much better than 5 % [two  
145 relative standard deviations (2 x RSD)].

### 146 3. Results

147 Analysis of the seventeen ureilites examined in this study involved three ICP-MS runs per sample: one  
148 complete run for each unleached and leached aliquot, and a supplementary one for each leached aliquot after  
149 REE separation and concentration, which always confirmed the previous complete run. The results are given  
150 in Table 2. For the leached samples (samples “R” in table 2), the reported REE abundances are those  
151 obtained after separation.

152 Our results are in good agreement with literature values (e.g., Boynton et al., 1976; Goodrich et al.,  
153 1991; Spitz and Boynton, 1991; Warren and Kallemeyn, 1992; Warren et al., 2006; Friedrich et al., 2010;  
154 Barrat et al., 2016). Peridotites are poor in lithophile trace elements, and ureilites are no exception. However,  
155 they display a wide range of abundances for these elements, as exemplified by La ranging from 0.28 to 22.6  
156 ng/g in the unleached samples. Results obtained with the leached samples duplicate those obtained with the  
157 unleached samples for most of the determined elements. The rationale for leaching the sample powders was to  
158 remove or reduce any traces of terrestrial alteration they might contain, particularly for the light-REE  
159 elements, and this point is discussed further below. A direct examination of Table 2 shows that Li, Sc Ti, V,  
160 Zn, Zr, Y and heavy REEs concentrations are very similar in the unleached and leached aliquots. P, Ga, Cu,  
161 Rb, Sr, Cs and light REE abundances are sometimes lower in the leached samples, and this could reflect  
162 either preferential dissolution of phases by HNO<sub>3</sub> (e.g., sulfides for Cu, schreibersite for P) or removal of a

163 terrestrial contaminant (e.g., La, Ce and Sr), possibly scavenged by the secondary Fe-hydroxides or adsorbed  
164 by the interstitial, fine-grained, C-rich material (Guan and Crozaz, 2000). In the following sections, we will  
165 focus our discussion on the classical incompatible trace elements.

## 166 **4. Discussion**

### 167 **4.1. Fingerprints of terrestrial weathering and how to remove them in ureilites**

168 The low incompatible trace element abundances found in ureilites make them especially sensitive to  
169 terrestrial weathering.

170 Indeed, many ureilites display marked light REE enrichments and distinctive V-shaped REE patterns  
171 (Fig. 2a) that indicate the involvement of components enriched in light REE, which were first thought to be  
172 indigenous to the ureilite parent body (e.g., Boynton et al., 1976), but were more likely introduced into the  
173 rocks during terrestrial residence (e.g., Guan and Crozaz, 2000). Two falls in particular display V-shaped  
174 REE patterns: Novo Urey (Boynton et al., 1976) and Haverö (Wänke et al., 1972). However, Novo Urey was  
175 not collected immediately after its fall, and terrestrial contamination easily explains its light-REE enrichment  
176 (Guan and Crozaz, 2000). The case of Haverö is more ambiguous because this meteorite was recovered  
177 shortly after its fall. One may suggest that it contains minute amounts of an indigeneous light-REE rich  
178 phase, such as titanite. Such light-REE rich phases are exceptional in ureilites (Guan and Crozaz, 2000), and  
179 this hypothesis is unlikely at best. Only 70 ng/g of La were measured in Haverö by Wänke et al. (1972), and  
180 we believe that contamination during the handling and processing of the meteorite is a more probable  
181 explanation.

182 The secondary light-REE enriched components can be removed in Antarctic ureilites by HNO<sub>3</sub> (e.g.,  
183 Boynton et al., 1976; Spitz and Boynton, 1991). Leaching procedures are difficult to test for samples  
184 available in very small quantities: if the leaching is too weak, the secondary component is not totally  
185 eliminated; if the leaching is too strong, the compositions of the residues could be controlled by those of the  
186 most resistant phases, and could be very different to those of the pristine rocks. Because our allocated  
187 samples were small, it was not possible to completely evaluate the effectiveness of the various leaching  
188 procedures. After a few preliminary tests using strongly weathered Saharan ureilites, we concluded that a  
189 leaching step with 4 N HNO<sub>3</sub> for half an hour at room temperature, does not alter the pyroxene/olivine ratios  
190 in the residues, and so provides satisfactory results. The lithophile trace element abundances of the residues  
191 are often very similar to those of the unleached samples but the irregularities displayed by the REE patterns  
192 of the unleached samples (e.g., the Ce anomalies, see Fig. 2a) are erased or reduced. As exemplified by  
193 NWA 8049, a longer leaching duration does not produced very different results, and seems unnecessary  
194 (Table 2).

195 For each sample, the residues display lower La/Sm ratios than the unleached powders, which indicates  
196 that all the samples contained traces of a secondary light-REE enriched components (Fig. 2b). Only two

197 residues (ALH 81101 R1 and LAP 03587 R1) display patterns with slight La or Ce irregularities, suggesting  
198 a “residual” contribution of secondary light-REE enriched components, which should not be  
199 overemphasized. It is important to note that ureilites do not contain phosphates. P is largely controlled by  
200 phosphides that are devoid of REEs. The partial dissolution of phosphides by HNO<sub>3</sub> (Table 2), has obviously  
201 no impact on the incompatible trace element abundances of interest, except of course for P. The situation  
202 would be different for phosphate-bearing achondrites for which such a leaching procedure is not suitable and  
203 is not recommended. We leached MET 01085 more severely because this rock is a pyroxenite and the  
204 possible preferential dissolution of olivine was not a problem.

205 The lithophile trace element abundances of the residues are certainly very close to those of the pristine  
206 ureilites. Indeed, the REE abundances in the residues are very similar to those measured in the fresh  
207 Almahata Sitta ureilites (Fig. 3). Only these data and the P abundances of the unleached fractions will be  
208 used in the following sections and drawn in the various figures. In contrast with Antarctic samples, the hot  
209 desert finds contained secondary phases such as barite, which are not easily leachable and account for high  
210 Ba and Sr abundances and sometimes anomalous REE distributions (e.g., Barrat et al., 2010). Therefore,  
211 only two mildly weathered Saharan ureilites were selected for this study.

#### 212 **4.2. Diversity of incompatible trace element abundances and ratios in ureilites**

213 The diversity of the trace element abundances in ureilites are well illustrated by their trace element  
214 patterns normalized to CI (Figs. 3 and 4). The range of abundances is huge, with values that are spread over  
215 two orders of magnitude for the most incompatible elements (e.g., Rb, Ba, La). The REE patterns display  
216 variable light REE depletions [e.g., (La/Sm)<sub>n</sub> = 0.022-0.65, (Pr/Sm)<sub>n</sub> = 0.11-0.73] and heavy-REE enrichments  
217 [(Dy/Lu)<sub>n</sub> = 0.18-0.62] and always show marked negative Eu anomalies (Eu/Eu\* = 0.14-0.68). These  
218 anomalies are accompanied by low Zr/Eu\* and Sr/Eu\* ratios [(Zr/Eu\*)<sub>n</sub> = 0.03-0.75, (Sr/Eu\*)<sub>n</sub> = 0.08-0.60,  
219 except NWA 8049 whose Sr/Eu\* ratio is explained by hot desert weathering]. Interestingly, a positive Eu  
220 anomaly and high (Sr/Eu\*)<sub>n</sub>, (Zr/Eu\*)<sub>n</sub> ratios were previously observed in ALM-A, a trachyandesitic clast  
221 collected in the Almahata Sitta strewnfield (Bischoff et al., 2014).

222 The trace element patterns allow us to distinguish two groups of ureilites. The first group (group A)  
223 comprises: A 881931, ALH 77257, ALH 81101, EET 96042, GRA 95205, GRO 95575, LAP 03587, PCA  
224 82506, Y 790981, Y 981810 and NWA 8049. The second group (group B) comprises: ALH 82130, EET  
225 83225, LAR 04315, Y 791538, and NWA 7686. Compared to group A, group B ureilites tend to be richer in  
226 heavy REEs, more light-REE depleted, and display among the lowest (Sr/Eu\*)<sub>n</sub>, (Zr/Eu\*)<sub>n</sub> ratios and deepest  
227 Eu anomalies. This separation in to two groups may appear somewhat arbitrary as the range of their  
228 respective trace element ratios display some overlap (e.g., Fig. 5). Nonetheless, the ureilites from these two  
229 groups are well separated in a (Dy/Lu)<sub>n</sub> vs. Eu/Eu\* plot (Fig. 5) or in (Pr/Sm)<sub>n</sub> or Eu/Eu\* vs. Sm plots (Fig.  
230 6). The MET 01085 pyroxenite exhibits a trace element pattern very similar to the group B ureilites, and so is  
231 most likely a member of this group.



232 The  $\text{Eu}/\text{Eu}^*$ ,  $(\text{Sr}/\text{Eu}^*)_n$  and  $(\text{Zr}/\text{Eu}^*)_n$  ratios are strongly correlated. In  $(\text{Sr}/\text{Eu}^*)_n$  and  $(\text{Zr}/\text{Eu}^*)_n$  vs.  
233  $\text{Eu}/\text{Eu}^*$  plots, our analyses display well defined trends which can be extended through the chondritic  
234 reference and up to ALM-A (Fig. 5). Similarly, the Eu anomalies of the ureilites are well correlated with  
235 their light-REE depletions, and a clear trend is obtained in a  $(\text{Pr}/\text{Sm})_n$  vs  $\text{Eu}/\text{Eu}^*$  plot, that extends to the  
236 chondritic ratios but not to ALM-A. The behavior of the heavy REEs seems more complex and a broad trend  
237 is only obtained for the group A ureilites in a  $(\text{Dy}/\text{Lu})_n$  vs.  $\text{Eu}/\text{Eu}^*$  plot (Fig. 5). We noticed that the poorer a  
238 ureilite is in incompatible trace elements (as exemplified by Sm), the more it is enriched in heavy-REE (Fig.  
239 6). No relationships are evident between Eu-anomalies, light-REE depletions and incompatible trace element  
240 abundances (Fig. 6). Collectively, these observations support the view that the ureilites represent mantle  
241 restites, but also point to the complexity of the melting and melt segregation processes, which can be further  
242 evaluated using trace element systematics.

243

#### 244 **4.3. Partial melting in the UPB body**

245 Various partial melting models have been tentatively proposed to explain the REE abundances of  
246 ureilites (e.g., Warren and Kallemeyn, 1992; Goodrich et al., 2007), but these do not provide a good match  
247 for the fine structures the REE patterns (see Fig. 16 in Goodrich et al., 2007).

248

249 The recent discovery of felsic brachinites (Day et al., 2009), suggests that the crust of many small  
250 differentiated bodies could have been silica-rich instead of basaltic, as previously thought. Furthermore,  
251 recent experimental studies have shown that at low  $f\text{O}_2$  conditions (i.e., at IW or below), partial melting of a  
252 chondritic protolith can generate magmas characterized by high alkali and silica contents (Gardner-Vandy et  
253 al., 2014; Usui et al., 2015). Seen in this light, the feldspathic debris found in polymict ureilites (e.g., Ikeda  
254 et al., 2000; Cohen et al., 2004), and more importantly the discovery of a “large” ureilitic trachyandesite  
255 (Bischoff et al., 2014) demonstrate that such magmas were generated by the melting of the UPB. Indeed, as  
256 pointed out by Goodrich and Wilson (2013), the early magmatism produced on the UPB could have been  
257 largely trachyandesitic. The extraction of these melts from chondritic precursors would yield residues with  
258 low alkalis and superchondritic Ca/Al ratios, precisely matching some of the distinctive chemical features  
259 observed in the ureilites.

260

261 Assuming a chondritic composition for the UPB, we propose that its melting history can be summarized  
262 as having taken place in three principal stages:

263

264 *a/ melting of the sulfides at a temperature close to the troilite-metal eutectic and segregation of a small*  
265 *S-rich core before the onset of significant silicate melting; this step is required to explain the average  $\delta^{56}\text{Fe}$*   
266 *of the ureilites, that is significantly higher than that of chondrites (Barrat et al., 2015); it is in agreement with*  
267 *the marked S-depletions and the siderophile element abundances of the ureilites (e.g., Warren et al., 2006);*

268 this step would not have had an impact on the incompatible trace element distributions which are neither  
269 chalcophile nor siderophile. After core segregation, the ureilite precursors would have displayed flat REE  
270 patterns, but their incompatible trace element abundances were likely to have been higher than that of CIs,  
271 probably close to 2 x CI, as suggested by the Sc abundances (Fig. 4). For the following calculations, we will  
272 assume concentrations = 1.8 x CI at the end of this step;

273

274 *b/ first step of silicate melting, and formation of silica and alkali-rich melts;* the proportions of the  
275 phases that melted during this step are uncertain; we used proportions similar to the ALM-A trachyandesite  
276 mode and assumed that these proportions were constant throughout this step. This stage would have  
277 terminated when plagioclase became exhausted. At the end of this step, we have assumed that the residual  
278 pyroxene would have been pigeonitic.

279

280 *c/ second step of silicate melting, and melting of an ureilitic lithology;* the residual lithology after the  
281 previous step contained mainly olivine and pigeonite. The highest temperatures attained by the ureilitic  
282 lithologies are not easy to estimate but were probably largely below 1400 °C based on melting experiments  
283 of harzburgites conducted at low pressure (e.g., Klingenberg and Kushiro, 1996).

284

285 In order to better characterize the differentiation process, we need a quantitative model of melting.  
286 Melt/residue partition coefficients can be calculated if the proportions of the phases in the residue are known.  
287 Several options are possible: batch or fractional, equilibrium or disequilibrium. When a restricted number of  
288 elements are considered, the various models can fit the data within uncertainties, provided that appropriate  
289 values for the unconstrained parameters are selected. However, when a large number of elements with  
290 different properties are selected, some of the models must be rejected, which is the major merit of modeling.  
291 This is illustrated below.

292 Fractionation models can be evaluated using REEs. However, they depend on many parameters (e.g.,  
293 starting modal proportions in the ureilite precursors, melting proportions of the phases, partition coefficients)  
294 and assumptions, which are summarized in Tables 3 and 4. The mineralogical compositions of the chondritic  
295 precursors of the ureilites are among the most important parameters. Various models of partial melting of  
296 chondrites can be found in the literature, and usually invoke olivine-pyroxenes-plagioclase assemblages in  
297 agreement with the mineralogy of the least metamorphosed chondrites (type 3). However, the metamorphism  
298 of chondrites not only resulted in a coarsening of the textures but also led to the development of phosphate  
299 grains (merrillite and apatite), chiefly by oxidation of P, which would initially have been contained by metal,  
300 as first suggested by Ahrens (1970). REEs migrated into phosphates during metamorphism (e.g., Murrell and  
301 Burnett, 1983), and these phases usually dominate the budget of these elements when present: REE  
302 abundances in chondritic phosphates are generally high, often on the order of 100 x CI for merrillite (e.g.,  
303 Jones et al., 2014). Therefore, the presence of phosphates during the melting of the ureilite precursors cannot  
304 be neglected and needs to be fully evaluated in order to derive a realistic differentiation model for the

305 ureilites. In the following, we will consider three different assemblages with phases in chondritic  
306 proportions: one free of phosphate, an apatite-bearing source and a merrillite-bearing source. Because  
307 phosphates are easily melted, they certainly involved in during the formation of the silica and alkali-rich  
308 melts. We assume that they are totally consumed at the same time as plagioclase. The apatite partition  
309 coefficients we have used are those that were experimentally determined by Prowatke and Klemme (2006).  
310 Partition coefficients for merrillite are more uncertain, but are certainly much higher than those for apatite.  
311 We selected the apparent partition coefficients determined using a merrillite analysis obtained in a shergottite  
312 (Basu Sarbadhikari et al., 2009), that are consistent with the behavior of REEs in this phase (e.g., Jolliff et  
313 al., 1993). In addition, the Eu partition coefficients are generally dependent of the oxygen fugacity. During  
314 ureilite formation,  $fO_2$  was low (close to IW-2, and possibly lower, Goodrich et al., 2013b), and the  
315 behaviors of Eu and Sr were probably very similar. This is confirmed by the excellent correlation between  
316 Eu/Eu\* and Sr/Eu\* ratios (Fig. 5). Consequently, the Eu and Sr partition coefficients are likely to have been  
317 similar during the melting of the ureilite precursors.

318

319 We initially assume that the melts were efficiently extracted from their sources, and consequently the  
320 melting processes would be analogous to fractional melting (Goodrich et al., 2007). The results of our  
321 calculations are shown in Figure 7. Using our set of parameters, plagioclase is exhausted and consequently  
322 no longer present in the residue after 16.5 % of melting. The first important observation that emerges from  
323 our calculations is that the presence and the nature of the phosphate in the initial assemblage have a strong  
324 impact on the shapes of the REE patterns obtained for the residues. Fractional melting of a precursor devoid  
325 of phosphate (Fig. 7 at left), or containing apatite (Fig. 7 middle), cannot account for the REE abundances  
326 measured in ureilites. Thus, the REE pattern of the residue calculated at the end of the first step of silicate  
327 melting (red pattern “plagioclase out”) crosses the ureilite fields, which is inconsistent with the lack of  
328 plagioclase in ureilites. On the other hand, fractional melting of a merrillite-bearing source produces residues  
329 with REE abundances that resemble group B ureilites. However, the calculated residues are much more light-  
330 REE depleted than the actual group A ureilites. A possible explanation for this discrepancy could be a  
331 disequilibrium partitioning limited by slow diffusion in pyroxenes during fractional melt extraction, as  
332 proposed by Goodrich et al. (2007, 2013). We have evaluated this possibility using the equations for  
333 disequilibrium fractional melting given by Liang and Liu (2016). We calculated the residues of melting for a  
334 range of disequilibrium parameter values ( $\epsilon$ ) for the same three sources as above (phosphate free, apatite and  
335 merrillite-bearing). The results obtained for F (degree of melting experienced by the bulk solid) =0.2 are  
336 compared in Figure 8 with the compositions of the ureilites. Disequilibrium fractional melting can potentially  
337 explain the less-marked light REE depletions of the group A compared to the group B ureilites. However, it  
338 can only marginally account for the fine structure of the REE patterns. While this process cannot be firmly  
339 ruled out, other processes are possible, and we believe more likely. Thus, it is important to note that if a  
340 limited melt porosity developed during melting, then melting can no longer be considered to have been  
341 perfectly fractional. Dynamic melting is thus a more likely process (e.g., Zou, 1998). In Figure 8, we

342 calculate the residues obtained by dynamic melting with a critical mass porosity ( $\phi$ ) of 2 %. Residues  
343 obtained with the merrillite-bearing sources display REE abundances similar to those of the group A ureilites  
344 (Fig. 9). From this we conclude that the dynamic melting of a merrillite-bearing source with  $\phi$  ranging from  
345 0 (fractional melting) to a couple of percent, can perfectly explain the REE abundances of both groups of  
346 ureilites (Figs. 6, 7 and 9). This model is consistent with F values ranging from 0.17 to 0.28. We emphasize  
347 that these values are just indicative because they are model dependent. Calling for disequilibrium during  
348 partial melting is not necessary to explain the data, and in the absence of robust evidence looks more *ad hoc*  
349 than anything else.

350

351 Our new data and calculations have a number of important implications for the evolution of the ureilite  
352 parent body:

353 a) at least two types of magmas were generated by the partial melting of the UPB. When plagioclase was still  
354 present in the mantle, melts were probably aluminous; relics of these melts are rare and are at present limited  
355 to the feldspathic debris found in polymict ureilites and to the ALM-A lava (e.g., Ikeda et al., 2000; Cohen et  
356 al., 2004; Bischoff et al., 2014). It is likely that these magmas were alkali and silica rich. The segregation of  
357 these melts would have removed most of the aluminum in the UPB mantle, and consequently most of its  
358  $^{26}\text{Al}$ , which is classically considered to provide the heat necessary for the melting of the small bodies.  
359 However, the exhaustion of  $^{26}\text{Al}$  from the residues did not turn off magma formation; further melting of the  
360 residues after the exhaustion of plagioclase would necessarily have produced a different type of melt,  
361 certainly Al-poor and nearly alkali-free, which has not yet been identified. According to the model  
362 calculations, the average degree of melting of ureilites is between 0.2 and 0.25, so that the mass of these Al  
363 and alkali-poor melts would have been about a third of that of the initial alkali and silica-rich magmas.

364 b) the bulk density at 1100°C of the ALM-A melt (calculated with the KWare Magma software) is 2.70  
365  $\text{g/cm}^3$ , and is lower than the average grain density of ureilites ( $3.35 \text{ g/cm}^3$ ) and carbonaceous chondrites  
366 ( $2.93 \text{ g/cm}^3$  for C2 chondrites,  $3.6 \text{ g/cm}^3$  for C3-4 chondrites) determined by Macke et al. (2011a,b).  
367 Consequently, these lavas reached the surface of the body. If volcanism was explosive, part of these melts  
368 could have been lost to space (e.g., Warren and Kallemeyn, 1992). However, the feldspathic clasts found in  
369 polymict ureilites (e.g., Ikeda et al., 2000; Cohen et al., 2004) and the ALM-A trachyandesite (Bischoff et  
370 al., 2014) unambiguously indicate that at least some (if not all) of these volcanics were retained by the body.  
371 As a consequence, at least part of the melts generated during the first step of silicate melting could have  
372 formed a crust at the surface of the UPB. The density of the second type of magma was likely to have been  
373 higher than that of the initial feldspathic melts. At present we do not know the exact compositions of these  
374 second stage melts and so it is not possible to estimate their density contrast with their ureilitic residues. We  
375 speculate that these melts were unlikely to have reached the surface of the UPB, especially if a  
376 trachyandesitic crust covered the body. The possibility that these low-Al melts were slightly denser than

377 ureilites, and could have formed an igneous layer below the ureilitic mantle requires further detailed  
378 evaluation.

379 c) the compositions of the olivine cores are not linked to the incompatible trace elements in ureilites (Fig.  
380 10). Both smelting and gasless melting of ureilitic precursors can explain the data. If the ureilite precursors  
381 were C-rich chondrites with rather homogeneous Mg# numbers, smelting would be required to generate the  
382 range of olivine compositions. In that case, this process was particularly complex and independent of the  
383 behavior of incompatible elements. On the other hand, gasless melting of precursors with various Mg#  
384 values is in perfect agreement with the decoupling between olivine core compositions and incompatible trace  
385 elements. It is noteworthy that ureilites with the highest Mg#s and the highest temperatures of equilibrium  
386 estimated from pigeonite compositions using the method of Singletary and Grove (2003) belong to group B  
387 and display among the highest Sm abundances (Fig. 10) or Yb abundances (Fig. 4). Consequently they are  
388 among the least residual samples, which is rather astonishing should they be the most smelted samples.  
389 Moreover, the temperatures of equilibrium calculated with pigeonite compositions are probably not good  
390 estimates of partial melting conditions. They more likely mirror subsolidus reequilibration temperatures and  
391 cannot be used to discuss the partial melting history of the ureilites.

392

## 393 **5. Conclusions**

394 The incompatible trace element systematics of 17 ureilites confirms that they are mantle restites. They  
395 display a wide range of incompatible trace element abundances and ratios, and among them, striking light  
396 REE depletions, negative Eu anomalies, low Zr/Eu\* and Sr/Eu\* ratios which are strongly correlated. Our  
397 modelling of the REE abundances shows that:

- 398 a) the REE abundances of the residues from a chondritic precursor depend strongly on the presence of  
399 phosphates; this remark is important not only for ureilites, but should be taken into account to  
400 explain the REE distributions of other types of achondrites, especially the primitive ones. We  
401 suggest that the chondritic precursors of ureilites contained REE-rich phosphates, chiefly merrillite;  
402 b) the REE abundances of the ureilites can be explained if at least two types of magmas were  
403 successively removed from their precursors. The first produced liquids consisted of aluminous melts  
404 whose existence is confirmed by feldspathic clasts known in polymict ureilites (e.g., Ikeda et al.,  
405 2000; Cohen et al., 2004) and by ALM-A, a trachyandesite found in the Almahata Sitta strewnfield  
406 (Bischoff et al., 2014). Partial melting continued after the exhaustion of plagioclase from the source,  
407 and REEs indicate that Al and alkali-poor melts were produced. Partial melting was near fractional  
408 to dynamic with melt porosities that did not exceed ca. a couple of percent.

409 Rocks formed from the low-Al, low-alkali magmas are totally unknown in the meteorite record, but  
410 our sampling of the UPB is far from being complete and representative. It would be interesting to

411 determine the compositions of such melts. Experimental melting of ureilitic assemblages should now be  
412 undertaken to determine these compositions and to estimate the buoyancy of these melts within the UPB.

413 The successive eruptions of trachyandesitic lavas would almost certainly have built up a crust on the  
414 surface of the UPB. The formation of such magmas in a C-rich body casts doubts on the arguments of  
415 Weiss and Elkins-Tanton (2013) and Fu and Elkins-Tanton (2014) who suggested that magmas  
416 generated by partial melting of carbonaceous chondrites and possibly ordinary chondrites, were too  
417 dense to ascend to the surface of their parent bodies. However, this interpretation was obtained using  
418 previous experimental results. Subsequently, recent studies have shown that the melting of chondrites  
419 can generate at low  $fO_2$ , silica and alkali enriched melts which are buoyant with respect to their  
420 precursors (Usui et al., 2015). Therefore, we suggest that the hypothesis of the preservation of a  
421 chondritic crust on some differentiated bodies needs a reappraisal. Clearly additional experimental work  
422 is required to explore the possible melting conditions and the diversity of magmas potentially generated  
423 by the various types of chondrites.

424

## 425 **Acknowledgements**

426 The ureilites from Antarctica were kindly provided by the Meteorite Working Group (NASA) and  
427 the National Institute of Polar Research, Tokyo. US Antarctic meteorite samples are recovered by the  
428 Antarctic search for Meteorites (ANSMET) program which has been funded by NSF and NASA, and  
429 characterized and curated in the Department of Mineral Sciences of the Smithsonian Institution and  
430 Astromaterials Curation Office at NASA Johnson Space Center. A dozen Saharan ureilites were generously  
431 provided by Bruno and Carine Fectay and Peter Marmet but the analyses were not integrated to this work  
432 because of their too-strong hot-desert flavors. The support of and discussions with Richard Greenwood are  
433 greatly acknowledged. We thank Christian Koeberl for the editorial handling, Hilary Downes and an  
434 anonymous reviewer for constructive comments, and Pascale Barrat for her help. This work was funded by  
435 grants from the Programme National de Planétologie (CNRS-INSU) to the first author. JAB dedicates this  
436 work to the memory of Guy Barrat, his father, who died in the spring of 2016.  
437

438

## **References**

- 439 Ahrens L.H. (1970) The composition of stony meteorites (VIII). Observations on fractionation between the L and the H chondrites.  
440 *Earth Planet. Sci. Lett.* **9**, 345-347.
- 441 Barrat J.A., Keller F., Amossé J., Taylor R.N., Nesbitt R.W., Hirata T. (1996). Determination of rare earth elements in sixteen silicate  
442 reference samples by ICP-MS after Tm addition and ion exchange separation. *Geostandards Newsletter* **20**, 1, 133-140.
- 443 Barrat J.A., Yamaguchi A., Zanda B., Bollinger C., Bohn M. (2010) Relative chronology of crust formation on asteroid 4-Vesta:  
444 Insights from the geochemistry of diogenites. *Geochim. Cosmochim. Acta.* **74**, 6218-6231.
- 445 Barrat J.A., Zanda B., Moynier F., Bollinger C., Liorzou C., and Bayon G. (2012) Geochemistry of CI chondrites: Major and trace  
446 elements, and Cu and Zn isotopes. *Geochim. Cosmochim. Acta* **83**, 79-92.
- 447 Barrat J.A., Zanda B., Jambon A., Bollinger C. (2014) The lithophile trace elements in enstatite chondrites. *Geochim. Cosmochim.*  
448 *Acta.* **128**, 71-94.
- 449 Barrat J.A., Rouxel O., Wang K., Moynier F., Yamaguchi A., Bischoff A., Langlade J. (2015) Early stages of core segregation  
450 recorded by Fe isotopes: insights from the ureilite meteorites. *Earth Planet. Sci. Lett.* **419**, 93-100.

- 451 Barrat J.A., Dauphas N., Gillet P., Bollinger C., Etoubleau J., Bischoff A., Yamaguchi A. (2016) Evidence from Tm anomalies for  
452 non-CI refractory lithophile element proportions in terrestrial planets and achondrites. *Geochim. Cosmochim. Acta*, **176**, 1-17.
- 453 Basu Sarbadhikari A, Day J.M.D., Liu Y., Rumble III D., Taylor L.A. (2009) Petrogenesis of olivine-phyric shergottite Larkman  
454 Nunatak 06319: Implications for enriched components in martian basalts. *Geochim. Cosmochim. Acta* **73**, 2190-2214.
- 455 Bischoff A., Horstmann M., Barrat J.A., Chaussidon M., Pack A., Herwartz D., Ward D., Vollmer C., Decker S. (2014)  
456 trachyandesitic volcanism in the early Solar System. *Proc. Natl. Acad. Sci. USA* **111**, 35, 12689-12692.
- 457 Boynton W.V., Starzyk P.M., and Schmitt R.A. (1976) Chemical evidence for the genesis of the ureilites, the achondrite Chassigny  
458 and the nakhlites. *Geochim. Cosmochim. Acta* **40**, 1439-1447.
- 459 Budde G., Kruijjer T.S., Fischer-Gödde M., Irving A.J., Kleine T. (2015) Planetary differentiation revealed by the Hf-W  
460 systematics of ureilites. *Earth Planet. Sci. Lett.* **430**, 316-325.
- 461 Carporzen L., Weiss B.P., Elkins-Tanton L.T., Shuster D.L., Ebel D.S., Gattacceca J. (2011) Magnetic evidence for a partially  
462 differentiated carbonaceous chondrite parent body. *Proc. Natl. Acad. Sci. USA* **108**, 6386-6389.
- 463 Clayton, R.N., Mayeda, T.K. (1996) Oxygen isotope studies of achondrites. *Geochim. Cosmochim. Acta* **69**, 1999-2017.
- 464 Cohen, B.A., Goodrich, C.A., Keil, K. (2004) Feldspathic clast populations in polymict ureilites: Stalking the missing basalts from  
465 the ureilite parent body. *Geochim. Cosmochim. Acta* **68**, 4249-4266.
- 466 Cournède C., Gattacceca J., Gounelle M., Rochette P., Weiss B.P., Zanda B. (2015) An early solar system magnetic field recorded in  
467 CM chondrites. *Earth Planet. Sci. Lett.* **410**, 62-74.
- 468 Day J.M.D., Ash R.D., Liu Y., Bellucci J.J., Rumble D. III, McDonough W.F., Walker R.J., and Taylor L.A. (2009) Early formation  
469 of evolved asteroidal crust. *Nature* **457**, 179-182.
- 470 Downes, H., Mittlefehldt, D.W., Kita, N.T., Valley, J.W. (2008) Evidence from polymict ureilite meteorites for a disrupted and re-  
471 accreted single ureilite parent asteroid gardened by several distinct impactors. *Geochim Cosmochim Acta* **72**, 4825-4844.
- 472 Evans T.M., St. C. O'Neill H., Tuff J. (2008) The influence of melt composition on the partitioning of REEs, Y, Sc, Zr and Al  
473 between forsterite and melt in the system CMAS. *Geochim. Cosmochim. Acta* **72**, 5708-5721.
- 474 Friedrich J.M., Wolf S., Rumble III D., Troiano J., Gagnon C.J.L., Compton J.R., Jenniskens P., Shaddad M.H. (2010) The elemental  
475 composition of Almahata Sitta. *Meteoritics Planet. Sci.* **45**, 1718-1727.
- 476 Fu R.R., Elkins-Tanton L.T. (2014) The fate of magmas in planetesimals and the retention of primitive chondritic crusts. *Earth*  
477 *Planet. Sci. Lett.* **390**, 128-138.
- 478 Gardner-Vandy K.G., McCoy T.J., Bullock E.S. (2014) Making evolved melts on asteroids. **45<sup>th</sup> Lunar Planet. Sci. Conf.**, #1483  
479 (abstract).
- 480 Goodrich C.A. (1992) Ureilites: A critical review. *Meteoritics* **27**, 327-352.
- 481 Goodrich C.A., Wilson L. (2013) Non-basaltic magmatism on the ureilite parent body. Workshop on Planetary Formation and  
482 Differentiation, # 8018 (abstract).
- 483 Goodrich C.A., Patchett P.J., Lugmair G.W., Drake M.J. (1991) Sm-Nd and Rb-Sr isotopic systematics of ureilites. *Geochim.*  
484 *Cosmochim. Acta* **55**, 829-848.
- 485 Goodrich, C.A., Wlotzka, F., Ross, D. K. and Bartoschewitz, R. (2006) NWA 1500: plagioclase-bearing monomict ureilite or  
486 ungrouped achondrite? *Meteorit. Planet. Sci.* **41**, 925-952 (2006).
- 487 Goodrich C.A., Van Orman J.A., Wilson L. (2007) Fractional melting and smelting on the ureilite parent body. *Geochim.*  
488 *Cosmochim. Acta* **71**, 2876-2895.
- 489 Goodrich C.A., Hutcheon I.D., Kita N.T., Huss G.R., Cohen B.A., Keil, K. (2010) <sup>53</sup>Mn-<sup>53</sup>Cr and <sup>26</sup>Al-<sup>26</sup>Mg ages of a feldspathic  
490 lithology in polymict ureilites. *Earth Planet. Sci. Lett.* **295**, 531-540.

- 491 Goodrich C.A., Wilson L., van Orman J.A., Michel P. (2013) Comment on “Parent body depth-pressure-temperature relationships  
492 and the style of the ureilite anatexis” by P. H. Warren (MAPS 47:209–227) *Meteoritics & Planetary Science* 48 1096-1106.
- 493 Goodrich C.A., Sutton S.R., Wirick S., Jercinovic M.J. (2013b) Chromium valences in ureilite olivine and implications for ureilite  
494 petrogenesis. *Geochim. Cosmochim. Acta* **122**, 280–305.
- 495 Goodrich C.A., Hartmann W.K., O’Brien D., Weidenschilling S.J., Wilson L., Michel P., Jutzi M. (2015) Origin and history of  
496 ureilitic material in the solar system: the view from asteroid 2008 TC3 and the Almahata Sitti meteorite. *Meteoritics Planet. Sci.*  
497 **50**, 782-809.
- 498 Greenwood, R.C., Franchi, I.A., Jambon, A., Buchanan, P. (2005) Widespread magma oceans on asteroidal bodies in the early solar  
499 system. *Nature* **435**, 916-918.
- 500 Guan Y., Crozaz G. (2000) Light rare earth element enrichments in ureilites: a detailed ion microprobe study. *Meteoritics Planet. Sci.*  
501 **35**, 131-144.
- 502 Ikeda Y., Prinz M., Nehru C.E. (2000) Lithic and mineral clasts in the Dar al Gani (DaG) 319 polymict ureilite. *Antarctic Meteorite*  
503 *Research* **13**, 177-221.
- 504 Jolliff, B.L., Haskin, L.A. Colson, R.O., and Wadhwa, M. (1993) Partitioning in REE-saturating minerals: Theory, experiment, and  
505 modelling of whitlockite, apatite, and evolution of lunar residual magmas. *Geochimica Cosmochimica Acta* **57**, 4069–4094.
- 506 Jones R.H., McCubbin F.M., Dreeland L., Guan Y., Burger P.V., Shearer C.K. (2014) Phosphate minerals in LL chondrites: A record  
507 of the action of fluids during metamorphism on ordinary chondrite parent bodies. *Geochim. Cosmochim. Acta* **132**, 120-140.
- 508 Klingenberg B.M.E.T., Kushiro I. (1996) Melting of a chromite-bearing harzburgite and generation of boninitic melts at low  
509 pressures under controlled oxygen fugacity. *Lithos* **37**, 1-13.
- 510 Liang Y, Liu B. (2016) Simple models for disequilibrium fractional melting and batch melting with application to REE fractionation  
511 in abyssal peridotites. *Geochim. Cosmochim. Acta* **173**, 181-197.
- 512 Macke R.J., Britt D.T., Consolmagno G.J. (2011a) Density, porosity, and magnetic susceptibility of achondritic meteorites.  
513 *Meteoritics Planet. Sci.* **46**, 311-326.
- 514 Macke R.J., Consolmagno G.J., Britt D.T. (2011b) Density, porosity, and magnetic susceptibility of carbonaceous chondrites.  
515 *Meteoritics Planet. Sci.* **46**, 1842-1862.
- 516 McKay G., Le L. and Wagstaff J. (1991) Constraints on the origin of the mare basalt europium anomaly: REE partition coefficients  
517 for pigeonite. *Lunar Planet. Sci.* **22**, 883–884.
- 518 Mittlefehldt D.W., McCoy T.J., Goodrich C.A., Kracher A. (1998) Non-chondritic me-teorites from asteroidal bodies. In: Papike, J.J.  
519 (Ed.), *Planetary Materials*. Mineralogical Society of America, Washington, DC, 195 pp.
- 520 Myamoto M., Takeda H., Toyoda H. (1985) Cooling history of some Antarctic ureilites. *J. Geophys. Res.* **90** (supplement), D116–  
521 D122.
- 522 Murrell M.T., Burnett D.S. (1983) The behavior of actinides, phosphorus, and rare earth elements during chondrite metamorphism.  
523 *Geochim. Cosmochim Acta* **47**, 1999-2014
- 524 Prowatke S., Klemme S. (2006) Trace element partitioning between apatite and silicate melts. *Geochim. Cosmochim. Acta* **70**, 4513-  
525 4527.
- 526 Rankenburg K., Humayun M., Brandon A. D., Herrin J.S. (2008) Highly siderophile elements in ureilites. *Geochim. Cosmochim.*  
527 *Acta* **72**, 4642–4659.
- 528 Scott, E.R.D., Taylor, G.J., Keil, K. (1993) Origin of ureilite meteorites and implications for planetary accretion. *Geophys. Res. Lett.*  
529 **20**, 415–418.
- 530 Severs M.J., Beard J.S., Fefele L., Hanchar J.M., Mutchler S.R., Bodnar R.J. (2009) Partitioning behavior of trace elements between  
531 dacitic melt and plagioclase, orthopyroxene, and clinopyroxene based on laser ablation ICPMS analysis of silicate melt  
532 inclusions. *Geochim. Cosmochim. Acta* **73**, 2123-2141



- 533 Shimizu H., Masuda A. (1981) REE, Ba, Sr and Rb abundances in some unique Antarctic achondrites. *Memoirs of the National*  
534 *Institute of Polar Research, Tokyo, Special Issue n°20*, 211-219.
- 535 Singletary, S. J. and Grove, T. L. (2003) Early petrologic processes on the ureilite parent body. *Meteorit. Planet. Sci.* **38**, 95–108.
- 536 Spitz A.H., and Boynton W.V. (1991) Trace element analysis of ureilites: new constraints on their petrogenesis. *Geochim.*  
537 *Cosmochim. Acta* **55**, 3417–3430.
- 538 Takeda H. (1987) Mineralogy of Antarctic ureilites and a working hypothesis for their origin and evolution. *Earth Planet. Sci. Lett.*  
539 **81**, 358-370.
- 540 Usui T., Jones J.H., Mittlefehldt D.W. (2015) A partial melting study of an ordinary (H) chondrite composition with application to  
541 the unique achondrite Graves Nunataks 06128 and 06129. *Meteoritics Planet. Sci.* **50**, 759-781.
- 542 Van Orman J.A., Grove T.L., Shimizu (2001) Rare earth element diffusion in diopside: influence of temperature, pressure and ionic  
543 radius, and an elastic model for diffusion in silicates. *Contrib. Mineral. Petrol.* **141**, 687-703.
- 544 Wänke H., Baddenhausen H., Spettel B., Teschke F., Quijana-Rico M., Dreibus G., and Palme H. (1972) The chemistry of Haverö  
545 ureilite. *Meteoritics* **7**, 579-590.
- 546 Warren P.H. (2011) Stable isotopes and the noncarbonaceous derivation of ureilites, in common with nearly all differentiated  
547 planetary materials. *Geochim. Cosmochim. Acta* **75**, 6912-6926.
- 548 Warren P. H. (2012) Parent body depth-pressure-temperature relationships and the style of the ureilite anatexis. *Meteoritics &*  
549 *Planetary Science* **47**, 209–227.
- 550 Warren P. H. and Huber H. (2006) Ureilite petrogenesis: A limited role for smelting during anatexis and catastrophic disruption.  
551 *Meteorit. Planet. Sci.* **41**, 835–849.
- 552 Warren P. H. and Kallemeyn G. W. (1992) Explosive volcanism and the graphite-oxygen fugacity buffer on the parent asteroid(s) of  
553 the ureilite meteorites. *Icarus* **100**, 110–126.
- 554 Warren, P. H. and Rubin, A. E. (2010) Pyroxene-selective impact smelting in ureilites. *Geochim. Cosmochim. Acta* **74**, 5109–5133.
- 555 Warren, P.H., Ulf-Moller, F., Huber, H., Kallemeyn, G.W. (2006) Siderophile geochemistry of ureilite: a record of early stages of  
556 planetesimal core formation. *Geochim. Cosmochim. Acta* **70**, 2104-2126.
- 557 Weiss B.P., Elkins-Tanton L.T. (2013) Differentiated planetesimals and the parent bodies of chondrites. *Annu. Rev. Earth Planet.*  
558 *Sci.* **41**, 529-560.
- 559 Wilson L., Goodrich C.A., van Orman J.A. (2008) Thermal evolution and physics of melt extraction on the ureilite parent body.  
560 *Geochim. Cosmochim. Acta* **72**, 6154–6176.
- 561 Yamakawa A., Yamashita K., Makashima A. and Nakamura E. (2010) Chromium isotope systematics of achondrites: chronology and  
562 isotopic heterogeneity of the inner solar system. *Astrophys. J.* **720**, 150–154.
- 563 Zou H. (1998) Trace element fractionation during modal and nonmodal dynamic melting and open-system melting: A mathematical  
564 treatment. *Geochim. Cosmochim. Acta* **62**, 1937-1945.
- 565

566 Table 1. Details of meteorite samples studied. Olivine compositions are from Downes et al. (2008)<sup>D</sup>, Warren  
 567 and Rubin (2010)<sup>WR</sup>, and Barrat et al. (2015)<sup>B</sup>.

568

	source	mass	olivine core Fo%	Remarks
<b><i>Antarctica</i></b>				
A 881931,71	NIPR	0.5 g	78.7 <sup>B</sup>	
ALH 77257,105	NIPR	0.5 g	86.1 <sup>D</sup>	
ALH 81101,63	MWG	1.3 g	78.9 <sup>D</sup>	
ALH 82130,43	MWG	0.8 g	95.2 <sup>D</sup>	
EET 83225,37	MWG	0.8 g	88.3 <sup>D</sup>	
EET 96042,48	MWG	1.2 g	81.3 <sup>D</sup>	
GRA 95205,64	MWG	1.2 g	79.2 <sup>D</sup>	
GRO 95575,46	MWG	1.3 g	78.6 <sup>D</sup>	
LAP 03587,10	MWG	0.8 g	74.7 <sup>WR</sup>	
LAR 04315,46	MWG	0.8 g	81.9 <sup>WR</sup>	
MET 01085,23	MWG	0.7 g	no olivine	px Mg#=88.8 <sup>D</sup>
PCA 82506,125	MWG	1.4 g	79.2 <sup>D</sup>	
Y 790981,85	NIPR	0.6 g	77.5 <sup>D</sup>	
Y 791538,109	NIPR	0.5 g	91.3 <sup>D</sup>	
Y 981810,76	NIPR	0.5 g	78.3 <sup>B</sup>	
<b><i>Sahara</i></b>				
NWA 7686	JAB	1.8 g	91.0 <sup>B</sup>	
NWA 8049	JAB	2.0 g	84.3 <sup>B</sup>	

569

570

Table 2. Trace element abundances in unleached fractions (U) and residues after leaching (R1, R2, R3, see the text for details) of ureilites.

		A	A	ALH	ALH	ALH	ALH	ALH	ALH	EET	EET	EET	EET	GRA	GRA	GRO	GRO	GRO	LAP	LAP
		881931	881931	77257	77257	81101	81101	82130	82130	83225	83225	96042	96042	95205	95205	95575	95575	95575	03587	03587
		U	R1	U	R1	U	R1	U	R1	U	R1	U	R1	U	R1	U	R1a	R1b	U	R1
CaO	wt%		1.67		0.91		0.96		2.62		2.32		1.42		0.63		1.56	1.47		0.71
Li	µg/g	1.78	1.44	1.43	1.46	1.88	1.69	1.3	1.4	0.86	0.91	1.92	1.84	1.66	1.74	1.71	1.94	1.79	1.71	1.78
P	µg/g	189	147	235	199	90	82	335	255	501	411	379	301	263	219	310	253	266	170	152
Sc	µg/g	9.08	10.25	7.06	7.13	7.42	6.83	11.32	12.63	13.83	14.03	8.68	8.78	6.67	6.79	8.61	9.37	9.04	7.32	7.77
Ti	µg/g	201	206	120	120	89.3	73.8	335	378	274	276	201	199	125	124	123	148	139	61.3	69.3
V	µg/g	97	91	91	92	86	82	116	113	106	112	96	96	82	84	96	103	101	88	89
Cu	µg/g	9.33	7.31	2.51	2.05	6.16	4.02	5.28	3.07	2.27	1.59	8.91	5.71	4.34	2.67	3.32	2.12	2.59	5.03	3.82
Zn	µg/g	240	198	204	212	114	110	180	193	99	107	221	220	154	146	130	139	133	238	233
Ga	µg/g	2.16	2.08	1.64	1.37	1.25	0.87	2.55	1.14	1.55	1.3	2.56	1.73	1.78	1.37	1.64	1.36	1.49	1.33	1.09
Rb	ng/g	96	85	3.1	4.9	7	6.4	12	14	5.3	1.8	38	42	40	42	7.4	5.9	12	17	8.8
Sr	ng/g	704	623	42	35	21	11	456	504	137	126	444	413	209	178	20	25	16	135	57
Y	ng/g	465	465	152	151	106	102	755	859	670	677	383	404	209	212	104	113	112	98	102
Zr	ng/g	258	224	26	25	15	12	145	157	20	19	113	119	131	124	11	10	11	24	21
Cs	ng/g	8.04	5.71	1.35	0.6	n.d.	4.61	1.11	0.85	0.51	0.33	2.61	5.45	2.37	4.37	0.47	n.d.	n.d.	1.53	0.98
Ba	ng/g	233	187	8.51	4.67	6.66	2.46	32.4	20.9	38.0	14.2	55.9	54.1	59.6	55.3	4.9	2.2	10.1	43.7	23.8
La	ng/g	18.6	14.0	0.80	0.59	0.64	0.22	8.32	7.76	1.42	0.69	5.98	5.27	6.01	4.94	0.28	0.25	0.13	3.81	1.28
Ce	ng/g	46.8	35.2	3.47	1.88	1.78	0.74	31.2	31.1	5.13	3.13	18.1	16.2	15.6	13.3	1.12	0.68	0.40	8.63	3.18
Pr	ng/g	7.69	6.00	0.52	0.38	0.22	0.093	7.68	7.51	1.71	1.33	3.34	3.28	2.52	2.22	0.12	0.12	0.076	1.13	0.45
Nd	ng/g	42.9	34.9	3.22	2.72	1.03	0.674	54.2	60.8	19.9	18.0	23.0	22.5	14.0	12.8	0.76	0.78	0.63	5.24	2.63
Sm	ng/g	18.4	17.2	2.22	2.02	0.92	0.712	32.1	36.0	20.4	20.2	12.9	13.3	6.29	5.87	0.70	0.77	0.73	2.07	1.64
Eu	ng/g	5.29	4.67	0.56	0.337	0.137	0.118	3.81	4.39	1.76	1.60	3.04	3.10	1.85	1.67	0.169	0.176	0.157	0.44	0.49
Gd	ng/g	36.3	35.1	6.45	6.23	2.90	2.81	67.6	78.6	59.9	55.8	26.6	27.8	12	11.7	2.93	3.19	3.09	4.79	4.61
Tb	ng/g	8.51	8.31	1.95	1.85	0.97	0.959	15.2	17.4	13.8	13.1	6.3	6.47	2.92	2.84	0.95	1.08	1.06	1.21	1.31
Dy	ng/g	68.5	68.6	18.4	18.5	10.7	10.6	116	136	107	106	50.6	53	24.3	24.7	10.6	11.9	11.6	11.6	12.1
Ho	ng/g	18.3	18.2	5.79	5.64	3.46	3.43	28.8	34.6	27.3	27	13.1	13.8	6.81	6.85	3.38	3.87	3.74	3.41	3.57
Er	ng/g	61.9	61.9	22.5	22.6	15	14.3	96	111	89.5	85.2	44.8	47.5	25	25.3	14.6	16.2	15.9	13.7	14.1
Yb	ng/g	82.8	82.6	40.4	38.8	26.7	27.0	116	133	106	105	61.1	65.9	38.8	39.9	28.6	31.5	30.8	24.8	26.3
Lu	ng/g	14.4	14.0	7.52	7.20	5.37	5.36	18.9	21.5	17.7	16.6	10.9	11.5	7.16	7.31	5.91	6.37	6.15	4.99	5.26
(La/Sm) <sub>n</sub>		0.66	0.532	0.234	0.19	0.453	0.201	0.169	0.14	0.045	0.022	0.302	0.258	0.622	0.548	0.262	0.213	0.113	1.20	0.507
(Pr/Sm) <sub>n</sub>		0.702	0.587	0.391	0.317	0.397	0.22	0.402	0.35	0.141	0.111	0.436	0.415	0.675	0.637	0.298	0.255	0.175	0.919	0.458

(Dy/Lu) <sub>n</sub>	0.46	0.475	0.237	0.249	0.192	0.191	0.597	0.612	0.586	0.619	0.45	0.446	0.328	0.327	0.173	0.181	0.183	0.225	0.223
Eu/Eu*	0.619	0.576	0.446	0.288	0.253	0.254	0.248	0.250	0.152	0.144	0.497	0.489	0.643	0.611	0.357	0.339	0.316	0.428	0.540
(Sr/Eu*) <sub>n</sub>	0.625	0.582	0.252	0.225	0.29	0.18	0.225	0.217	0.09	0.086	0.552	0.495	0.55	0.493	0.319	0.361	0.243	0.984	0.479
(Zr/Eu*) <sub>n</sub>	0.504	0.460	0.348	0.359	0.466	0.442	0.157	0.148	0.028	0.029	0.308	0.314	0.76	0.754	0.381	0.330	0.370	0.386	0.392

Table 2 (continue)

		LAR	LAR	MET	MET	PCA	PCA	Y	Y	Y	Y	Y	Y	NWA	NWA	NWA	NWA	NWA
		04315	04315	01085	01085	82506	82506	790981	790981	791538	791538	981810	981810	7686	7686	8049	8049	8049
		U	R1	U	R3	U	R1	U	R1	U	R1	U	R1	U	R1	U	R1	R2
CaO	wt%		1.69		2.23		1.16		1.09		1.65		0.98		1.39		1.16	1.12
Li	µg/g	1.66	1.55	0.69	0.69	1.54	1.61	1.8	1.71	1.46	1.52	1.57	1.67	1.49	1.53	1.41	1.48	1.53
P	µg/g	257	255	506	182	270	220	337	284	546	401	276	223	526	474	261	230	233
Sc	µg/g	8.82	10.04	16.66	17.35	8.24	8.89	7.49	7.9	10.2	10.49	8.4	7.76	8.41	9.27	7.69	8.06	8.67
Ti	µg/g	167	199	556	590	141	154	163	161	297	298	138	119	204	224	112	117	126
V	µg/g	89	94	110	117	99	103	85	80	91	92	85	84	88	92	87	92	95
Cu	µg/g	7.33	5.65	5.18	1.96	3.29	2.29	12.55	9.71	3.82	2.93	11.38	9.13	5.54	3.76	4.2	1.82	1.51
Zn	µg/g	161	152	89	96	170	174	252	232	228	237	227	245	236	235	199	215	229
Ga	µg/g	1.96	1.31	2.95	2.43	2.02	1.72	2.39	2.06	2.51	1.76	1.72	1.23	2.47	2.12	1.57	1.34	1.39
Rb	ng/g	7.7	5.1	14	13	15	13	117	108	12	12	82	75	6.1	6.4	12	7.6	7.1
Sr	ng/g	121	113	645	525	65	59	785	727	148	144	519	396	224	235	132	177	172
Y	ng/g	298	345	1181	1188	164	172	425	424	542	534	293	248	375	420	167	165	169
Zr	ng/g	52	50	264	242	22	24	339	332	24	30	196	176	24	17	28	25	22
Cs	ng/g	0.77	0.65	1.13	0.82	n.d.	1.52	9.51	7.82	2.71	0.99	8.49	6.83	0.84	0.58	0.74	0.63	0.53
Ba	ng/g	5.64	7.69	113	39.7	9.66	7.34	295	233	19.7	14.3	201	124	13	10	392	80	83
La	ng/g	2.41	1.63	9.33	5.76	0.72	0.66	22.6	19.5	1.35	1.08	18.6	11.7	0.88	0.86	1.79	1.42	1.18
Ce	ng/g	7.45	6.25	31.6	22.1	3.17	2.1	55.3	48.9	5.72	4.09	47.1	30.8	4.26	3.85	4.9	3.99	3.49
Pr	ng/g	1.89	1.71	7.21	5.24	0.49	0.42	9.11	8.14	1.36	1.1	7.4	5.1	1.11	1.18	0.84	0.68	0.63
Nd	ng/g	14.6	15.8	52.6	44.5	2.98	2.95	49.2	46.3	11.3	10.8	37.9	28.6	10.7	12.1	4.65	4.21	3.96
Sm	ng/g	10.7	11.9	35.3	31.7	2.04	2.18	20.4	20.6	10.9	11.1	14.4	11.7	9.13	11.0	2.88	2.70	2.67
Eu	ng/g	1.21	1.31	6.45	5.23	0.56	0.592	6.39	6.27	1.53	1.40	4.05	3.30	1.94	2.11	0.52	0.644	0.603
Gd	ng/g	23.6	28.3	85.8	80.6	6.00	6.36	35.9	37.7	32.3	32.6	25.2	20.2	23.2	28.7	7.23	7.24	7.63
Tb	ng/g	5.35	6.68	20.8	20.5	1.79	1.90	8.01	8.3	8.73	8.76	5.48	4.43	6.01	7.23	2.35	2.06	2.14

Dy	ng/g	45.0	53.8	172	174	18.1	19.0	64.5	66.0	79.5	77.9	42.5	35.5	52.1	63.3	21.5	20.2	20.5
Ho	ng/g	11.6	14.1	44.6	46.3	5.48	5.81	15.9	16.8	21.3	21.4	11.0	9.19	14.6	17.3	6.37	6.04	6.18
Er	ng/g	40.4	47.1	159	159	21.7	23.1	54.7	56.4	74.4	75.3	38	32.2	50.6	60.8	24.7	23.6	23.8
Yb	ng/g	60.4	64.5	206	204	37.1	39.4	70.2	73.4	102	102	52.7	47.3	72.1	82.7	43.5	40.6	40.8
Lu	ng/g	11.4	11.1	34.1	33.1	7.17	7.43	11.8	12.5	17.4	17.3	9.65	8.60	13.1	14.1	8.30	7.62	7.68
(La/Sm) <sub>n</sub>		0.147	0.089	0.172	0.118	0.230	0.197	0.723	0.616	0.081	0.063	0.838	0.65	0.062	0.051	0.405	0.344	0.288
(Pr/Sm) <sub>n</sub>		0.297	0.243	0.343	0.278	0.401	0.324	0.752	0.663	0.209	0.167	0.863	0.732	0.204	0.182	0.489	0.427	0.395
(Dy/Lu) <sub>n</sub>		0.382	0.471	0.489	0.51	0.244	0.248	0.532	0.512	0.442	0.436	0.427	0.399	0.386	0.434	0.25	0.257	0.258
Eu/Eu*		0.231	0.217	0.355	0.314	0.484	0.482	0.716	0.681	0.246	0.224	0.644	0.65	0.404	0.361	0.345	0.441	0.404
(Sr/Eu*) <sub>n</sub>		0.175	0.142	0.269	0.239	0.424	0.362	0.667	0.599	0.181	0.174	0.626	0.592	0.354	0.305	0.664	0.918	0.873
(Zr/Eu*) <sub>n</sub>		0.167	0.137	0.242	0.242	0.323	0.331	0.632	0.601	0.064	0.080	0.519	0.576	0.082	0.049	0.304	0.282	0.244

---

Table 3. Starting modal compositions, and melting proportions (melting step, 1: with plagioclase; 2: after plagioclase exhaustion).

	olivine	orthopyroxene	clinopyroxene	pigeonite	plagioclase	apatite	merrillite
<b>starting compositions, step 1</b>							
phosphate-free source	53	31	5	0	11	0	0
apatite-bearing source	52.7	31	5	0	11	0.3	0
merrillite-bearing source	52.7	31	5	0	11	0	0.3
<b>melting proportions, step 1</b>							
phosphate-free source		13.9	19.4		66.7		
apatite-bearing source		12.1	19.4		66.7	1.82	
merrillite-bearing source		12.1	19.4		66.7		1.82
<b>melting proportions, step 2</b>							
	50			50			

Table 4. Mineral-melt partition coefficients and disequilibrium parameter used for calculations (melting step, 1: with plagioclase; 2: after plagioclase exhaustion). For each phase, the REE partition coefficients (except Eu) were recalculated using the best-fit order-3 polynome in a Log D vs. ionic radius plot from literature data (a : Evans et al., 2008 ; b : Severs et al., 2009 ; c : Prowatke and Klemme, 2006 ; d : Basu Sarbadhikari et al., 2009 ; e : McKay et al., 1991). The Eu and Sr partition coefficients were assumed to be similar during ureilite melting. This assumption is justified by the strong correlation between Eu/Eu\* and Sr/Eu\* (Fig. 5). The disequilibrium parameters for REE ( $\epsilon_{\text{REE}}$ ) are deduced from their diffusion parameters in diopside at 1200°C (Van Orman et al., 2001), with  $\epsilon_{\text{La}}$  fixed at 1.

	olivine	orthopyroxene	clinopyroxene	plagioclase	apatite	merrillite	pigeonite	$\epsilon_{\text{REE}}$
reference	a	b	b	b	c	d	e	
melting step	1, 2	1	1	1	1	1	2	1, 2
Sr	4.60E-05	0.003	0.101	2.42	4.3	2.73	0.002	
La	4.87E-06	0.003	0.082	0.087	10.99	68.6	0.0008	1.00
Ce	1.23E-05	0.0051	0.15	0.079	13.36	75.1	0.0017	0.914
Pr	3.00E-05	0.0088	0.249	0.068	15.15	79.4	0.0033	0.772
Nd	7.04E-05	0.0148	0.376	0.057	16.06	81.3	0.0056	0.609
Sm	2.94E-04	0.0355	0.635	0.037	15.29	79.2	0.0118	0.349
Eu	= $D_{\text{Sr}}$	= $D_{\text{Sr}}$	= $D_{\text{Sr}}$	= $D_{\text{Sr}}$	= $D_{\text{Sr}}$	= $D_{\text{Sr}}$	0.005	0.262
Gd	9.56E-04	0.0724	0.835	0.025	12.67	73.1	0.0203	0.193
Tb	0.0017	0.101	0.908	0.02	11.02	69.2	0.0262	0.140
Dy	0.00298	0.14	0.957	0.017	9.3	64.9	0.0338	0.101
Ho	0.00499	0.186	0.981	0.014	7.77	60.7	0.0433	0.0736
Er	0.00798	0.238	0.986	0.012	6.46	57.0	0.0550	0.0551
Tm	0.0122	0.295	0.978	0.011	5.38	53.6	0.0695	0.0424
Yb	0.0179	0.354	0.962	0.010	4.51	50.6	0.0873	0.0336
Lu	0.0251	0.414	0.942	0.009	3.82	48.1	0.109	0.0274

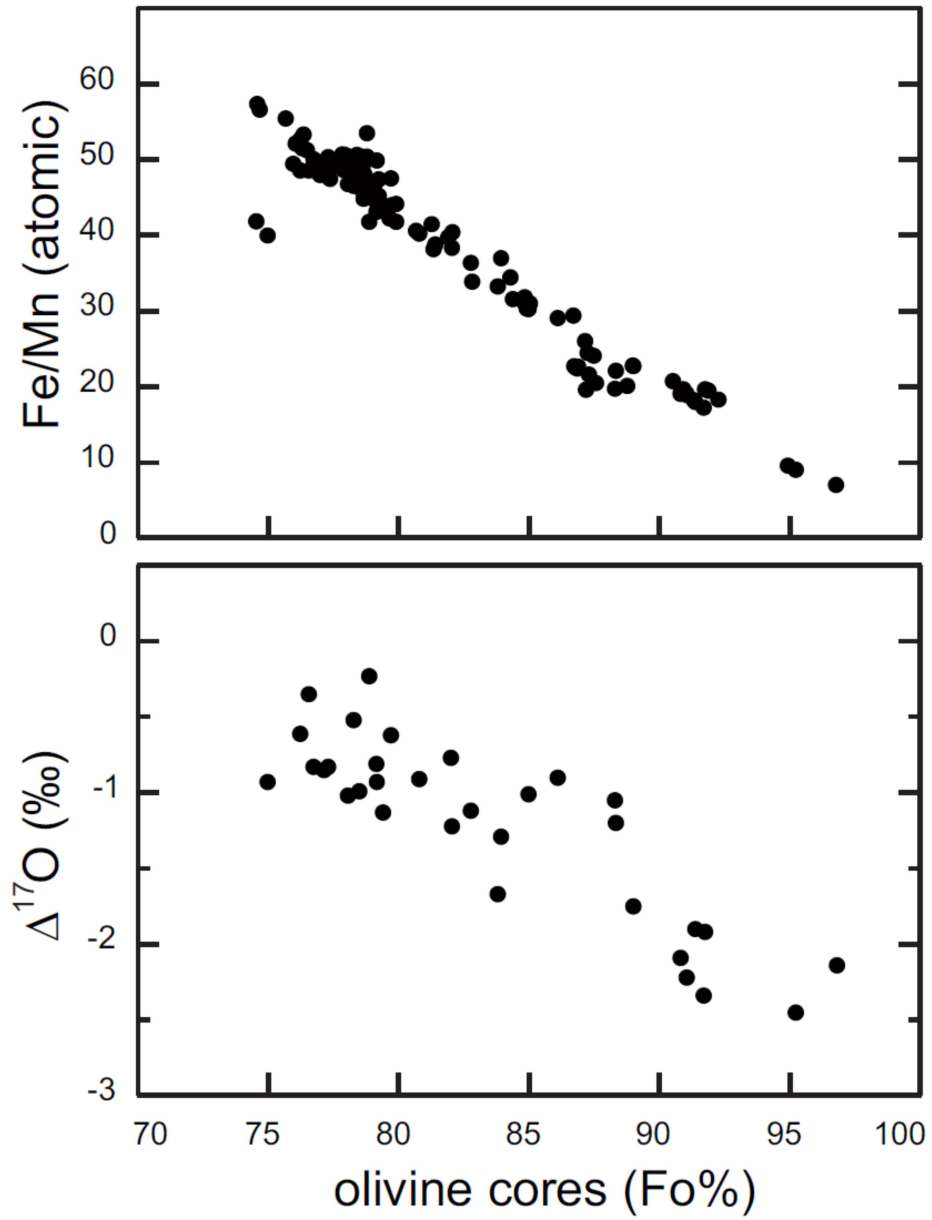


Figure 1. Plots of molar Fe/Mn ratios in olivine cores and  $\Delta^{17}\text{O}$  (Clayton and Mayeda, 1996) vs. the composition of the olivine cores (data mainly from Downes et al., 2008, Singletary and Grove, 2003, Goodrich et al., 2006; Barrat et al., 2015 and references therein).



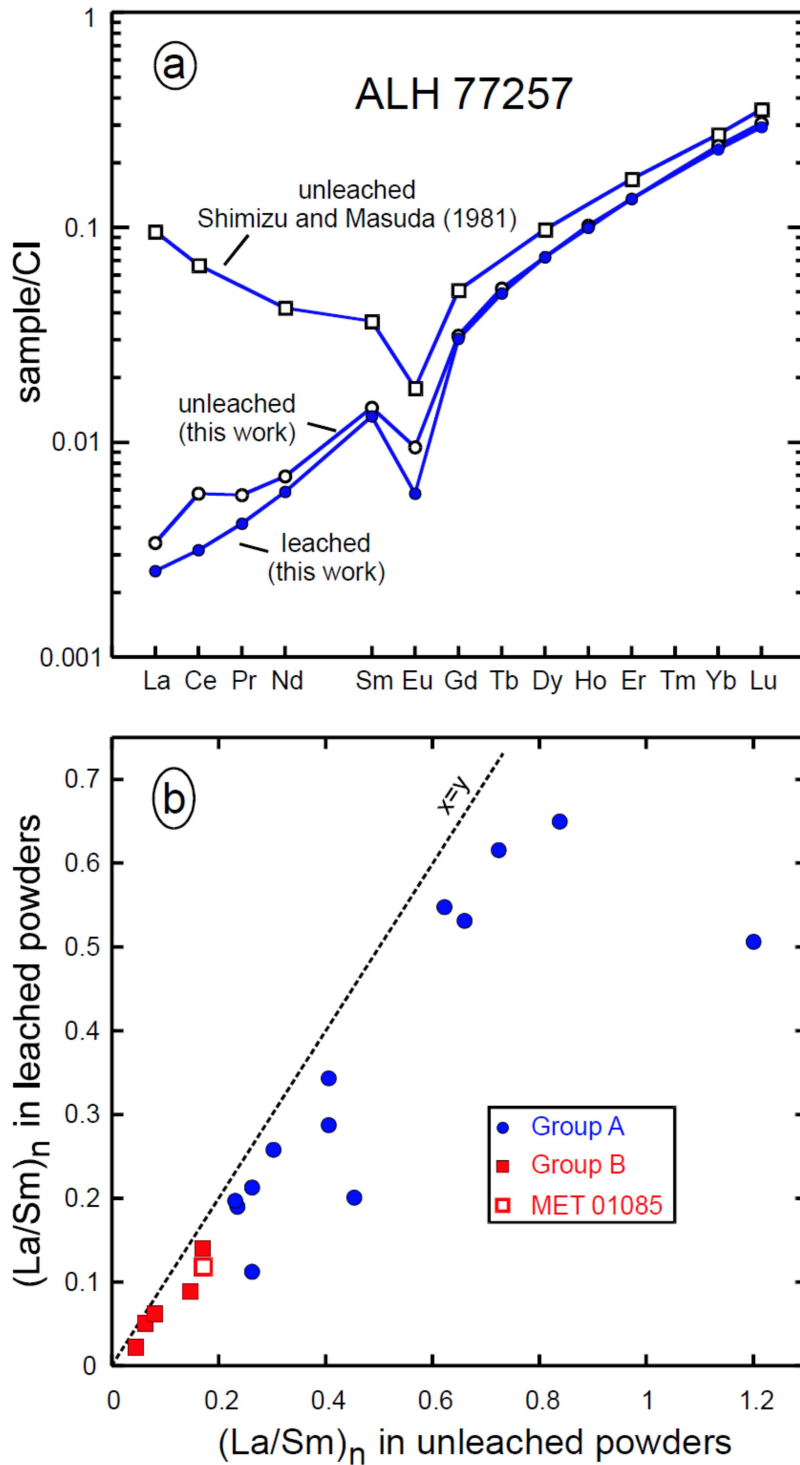


Figure 2. a) Selected REE patterns obtained for ALH 77257 normalized to CI chondrite (Barrat et al., 2012). Results obtained with unleached fractions display the fingerprints of a secondary component (positive Ce anomaly, light REE enrichment). These features are removed after leaching. Notice that the results obtained after leaching display the same Sm and heavy-REE abundances as the unleached powder (this work), and indicate that the residue is not pyroxene-enriched (no effect of selective dissolution of olivine). b)  $(La/Sm)_n$  ratios in the residues compared to the same ratios in the unleached powders. The residues display lower  $(La/Sm)_n$  ratios than the unleached powders, demonstrating that light-REE enriched secondary components were removed by the leaching step for all the samples.

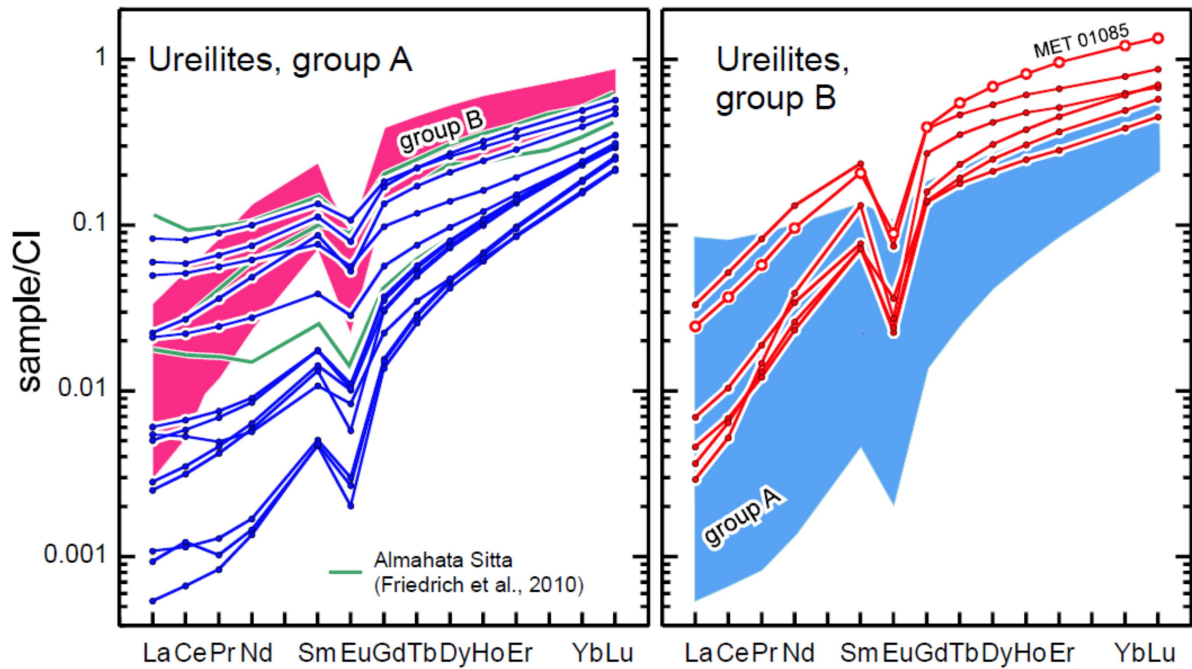


Figure 3. REE patterns of ureilites (leached samples), normalized to CI chondrite (Barrat et al., 2012). The patterns of three Almahata Sitta ureilites are shown for comparison (Friedrich et al., 2010).

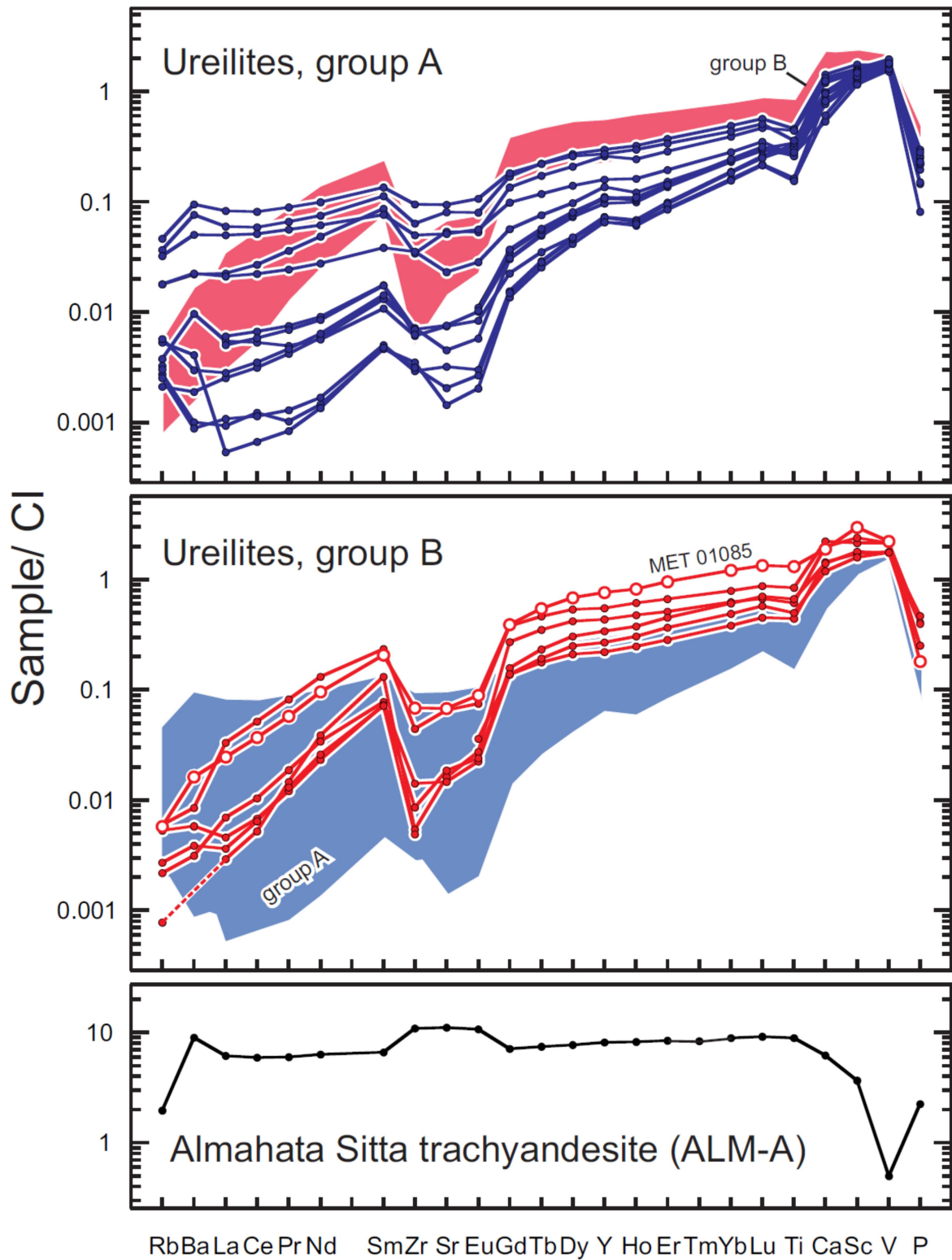


Figure 4. Trace element patterns of ureilites (concentrations obtained with the leached samples, except for P for which the concentrations in the unleached fractions were selected) and for the ALM-A trachyandesite (Bischoff et al., 2014) normalized to CI chondrite (Barrat et al., 2012). Ba and Sr abundances in the two Saharan samples have been omitted.

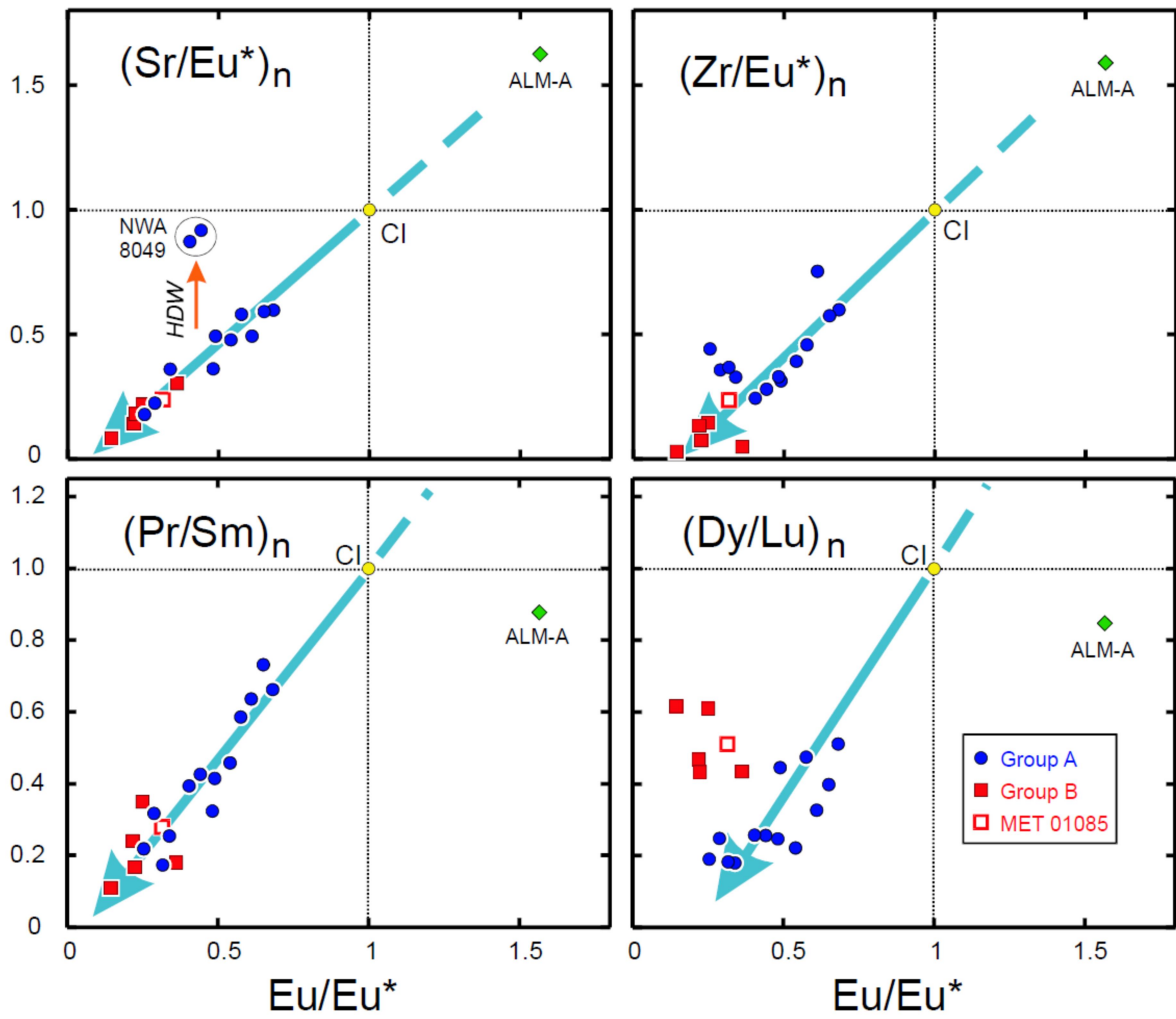


Figure 5.  $(\text{Sr}/\text{Eu}^*)_n$ ,  $(\text{Zr}/\text{Eu}^*)_n$ ,  $(\text{Pr}/\text{Sm})_n$ ,  $(\text{Dy}/\text{Lu})_n$  vs.  $\text{Eu}/\text{Eu}^*$  plots for ureilites (leached samples). Hot desert weathering (HDW) is responsible of the high  $\text{Sr}/\text{Eu}^*$  ratios displayed by NWA 8049.

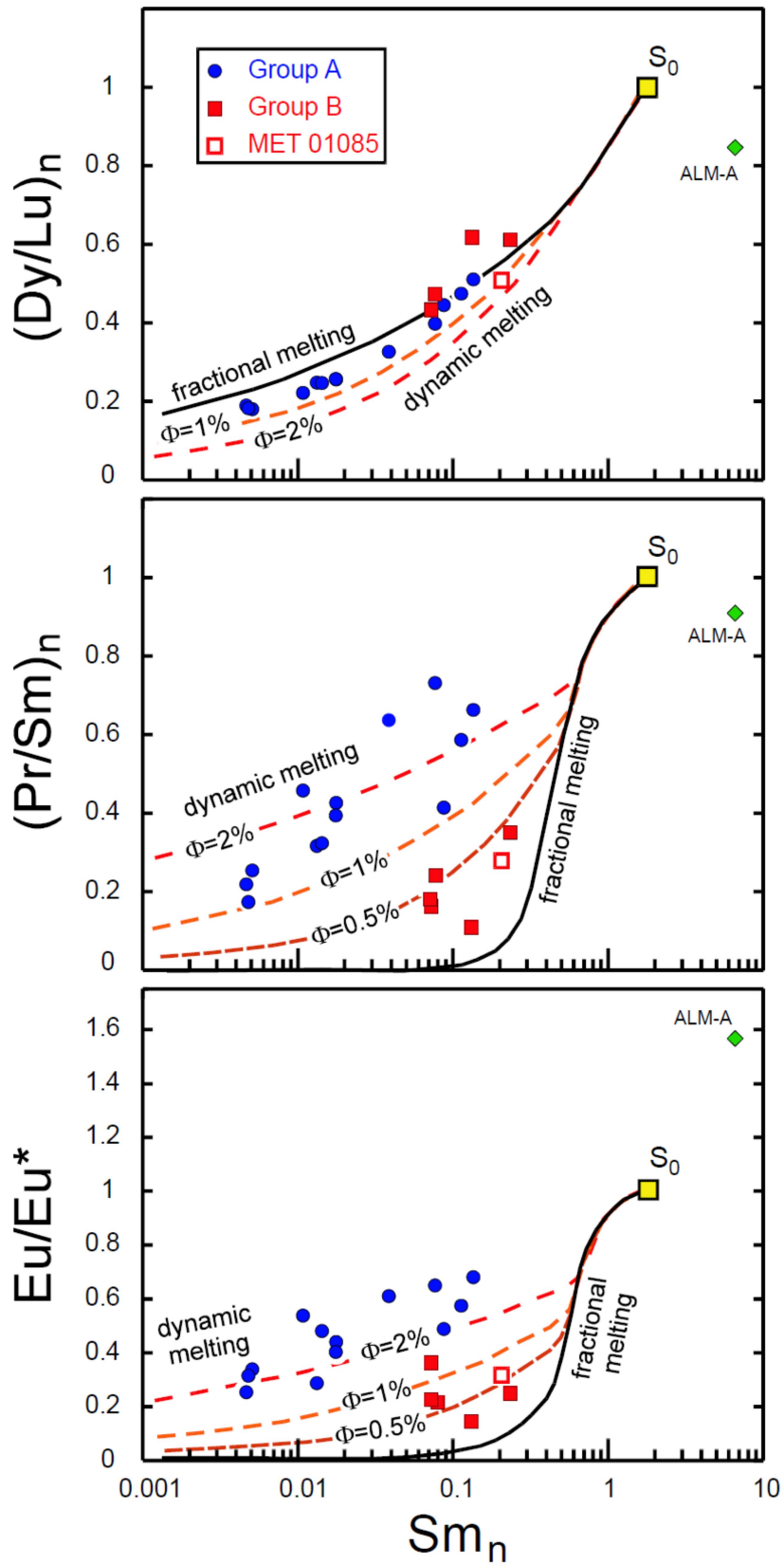


Figure 6.  $(Dy/Lu)_n$ ,  $(Pr/Sm)_n$ , and  $Eu/Eu^*$  vs.  $Sm_n$  plots for ureilites (leached samples). The partial melting curves obtained for a merrillite-bearing assemblage are shown for comparison.

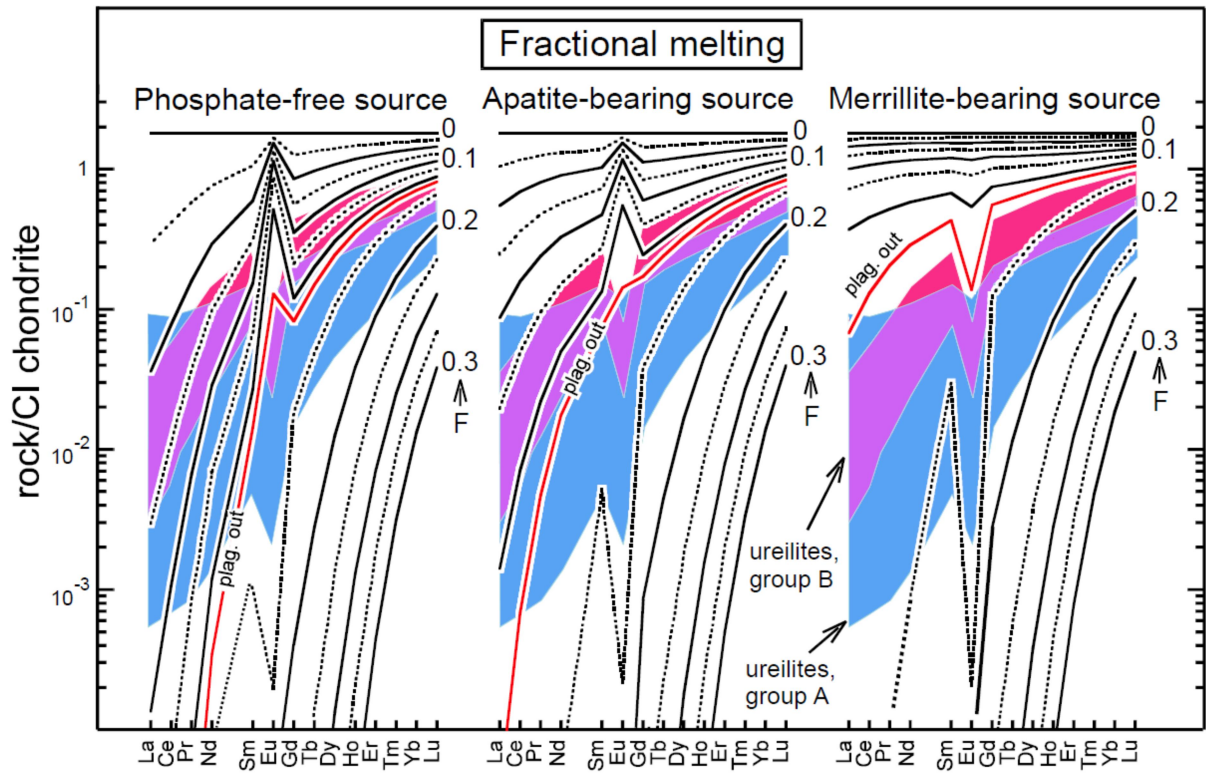


Figure 7. Results of REE modelling using three different ureilite precursors and the fractional melting law. The compositions of the sources, the melting proportions of the phases and the selected partition coefficients are given in Tables 3 and 4. The red pattern “plag. out” marks the end of the first step of silicate melting and the exhaustion of plagioclase. The fields for group A (blue) and group B (red) ureilites are shown for comparison.

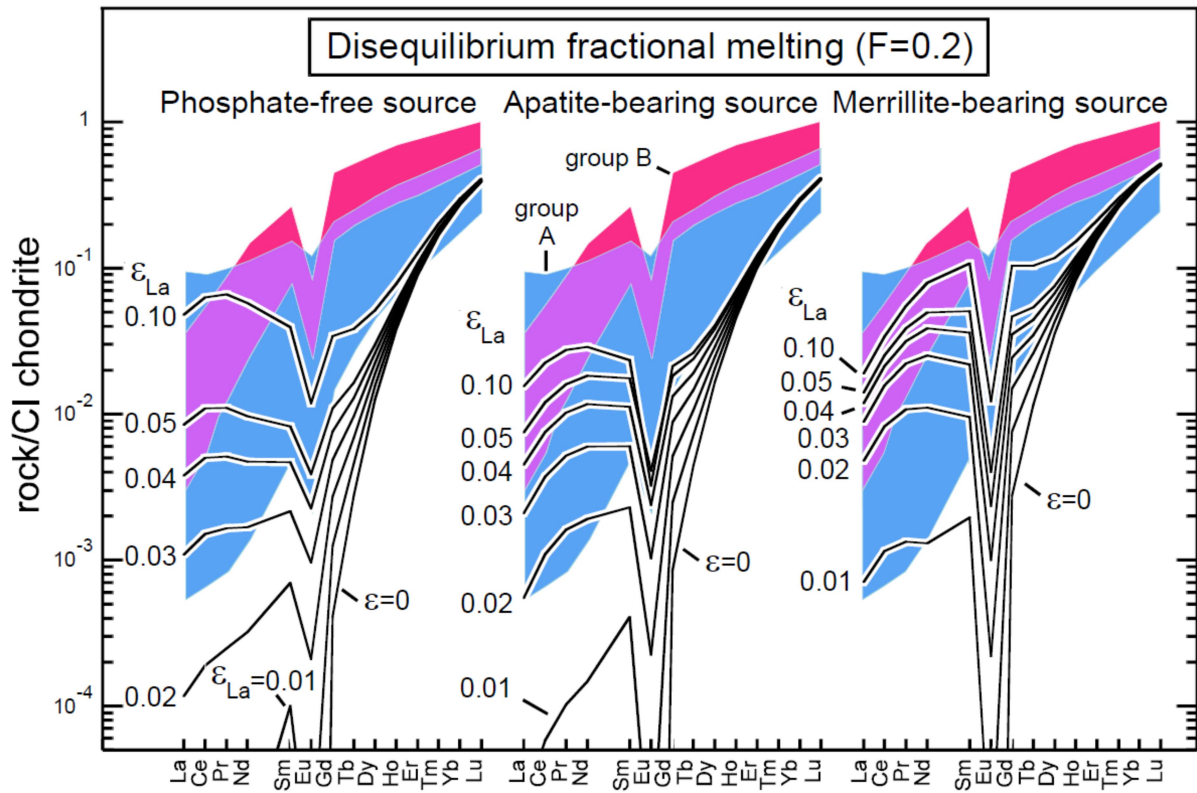


Figure 8. Results of REE modelling using three different ureilite precursors and a disequilibrium fractional melting law for  $F=0.2$ . The compositions of the sources, the melting proportions of the phases, the selected partition coefficients and the disequilibrium parameters are given in Tables 3 and 4. The fields for group A (blue) and group B (red) ureilites are shown for comparison.

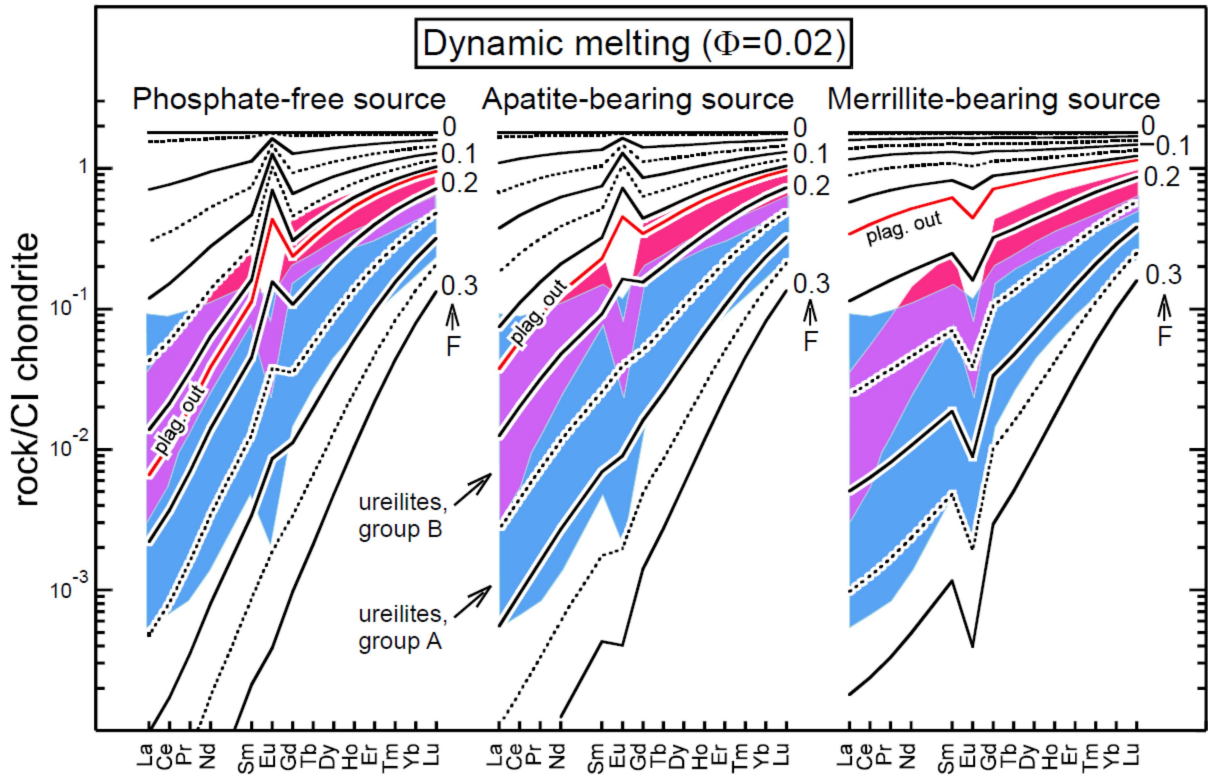


Figure 9. Results of REE modelling using three different ureilite precursors and assuming a dynamic melting model (Zou, 1998). The compositions of the sources, the melting proportions of the phases and the selected partition coefficients are given in Tables 3 and 4. The red pattern “plag. out” marks the end of the first step of silicate melting and the exhaustion of plagioclase. The fields for group A (blue) and group B (red) ureilites are shown for comparison.



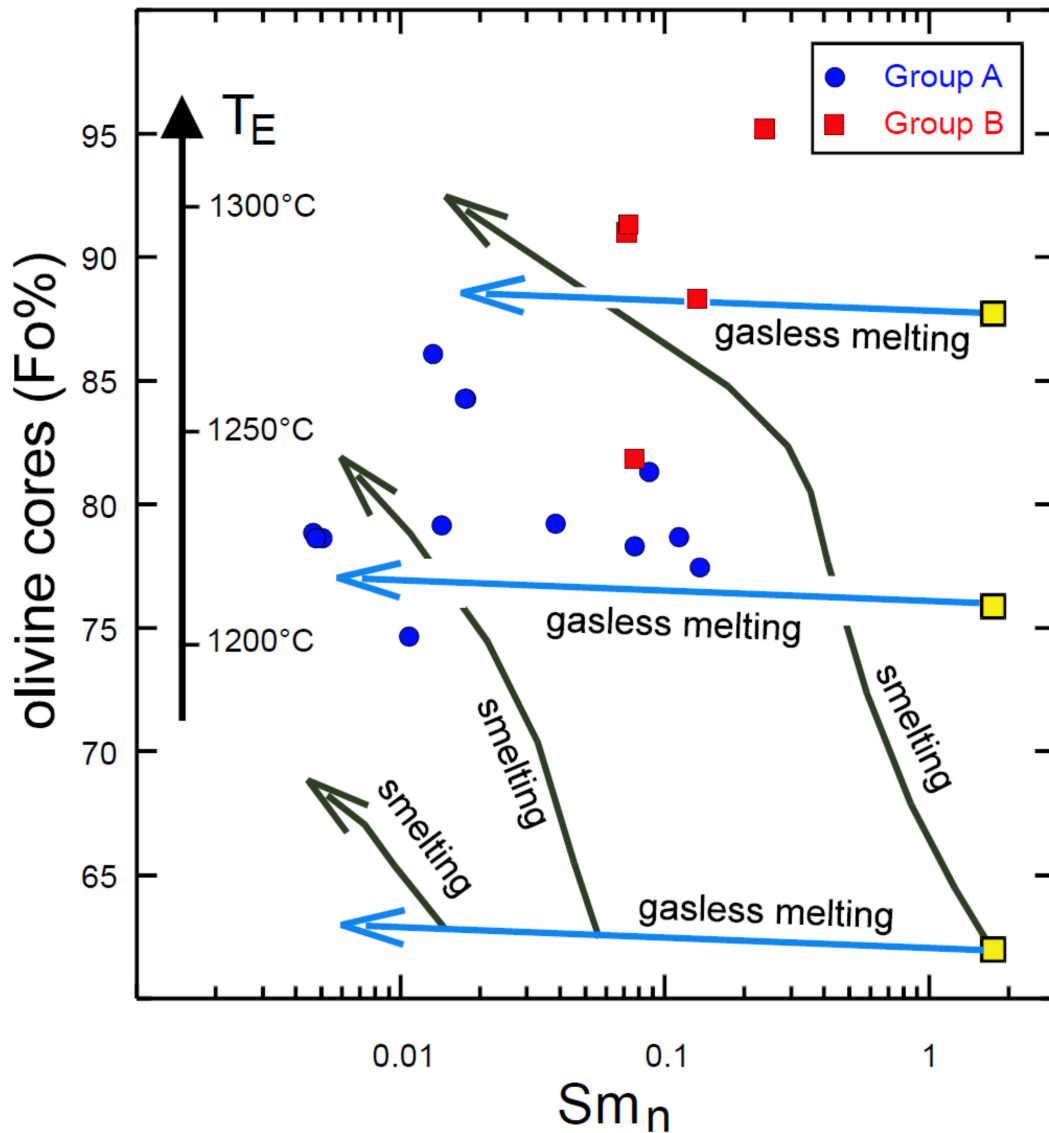


Figure 10. olivine core compositions vs. Sm abundances (normalized to CI) for ureilites (leached samples). Possible melting curves for smelting and gasless melting for three different hypothetical sources are shown for comparison. The vertical black arrow shows the evolution of the temperatures of equilibrium for ureilites estimated from pigeonite compositions using the method of Singletary and Grove (2003).